Neutrophils promote CXCR3-dependent itch in the development of atopic dermatitis

Authors and Affiliations: Carolyn M. Walsh[1‡], Rose Z. Hill[1‡], Jamie Schwendinger-Schreck[1], Jacques Deguine[1], Emily C. Brock[1], Natalie Kucirek[1], Ziad Rifi[1], Jessica Wei[2], Karsten Gronert[2], Rachel B. Brem[3,4], Gregory M. Barton[1], Diana M. Bautista[1,5]

1. Department of Molecular and Cell Biology, University of California, Berkeley, CA 94720, USA.
2. Vision Science Program, School of Optometry, University of California, Berkeley, CA 94720, USA.
3. Department of Plant and Microbial Biology, University of California, Berkeley, CA 94720, USA.
4. Buck Institute for Research on Aging, Novato, CA 94945, USA.
5. Helen Wills Neuroscience Institute, University of California, Berkeley, CA 94720, USA.

‡ These authors contributed equally to this work.

Abstract

Chronic itch remains a highly prevalent disorder with limited treatment options. Most chronic itch diseases are thought to be driven by both the nervous and immune systems, but the fundamental molecular and cellular interactions that trigger the early development of itch, and the acute-to-chronic itch transition, remain unknown. Here, we show that skin-infiltrating neutrophils are key initiators of itch behaviors in atopic dermatitis, the most prevalent chronic itch disorder. Neutrophil depletion significantly attenuated itch-evoked scratching behaviors in a mouse model of atopic dermatitis. Neutrophils were also required for several key hallmarks of chronic itch, including upregulation of inflammatory cytokines, skin hyperinnervation, enhanced expression of itch signaling molecules, and upregulation of activity-induced genes and markers of neuropathic itch. Finally, we demonstrate that induction of CXCL10, a ligand of the CXCR3 receptor that promotes itch via activation of sensory neurons, is neutrophil-dependent and that CXCR3 antagonism attenuates chronic itch.

Introduction

Chronic itch is a debilitating disorder that affects millions of people worldwide (Dalgard et al., 2015; Matterne et al., 2011; Mollanazar et al., 2016). It is a symptom of a number of skin diseases and systemic disorders, as well as a side effect of a growing list of medications. Like chronic pain, chronic itch can also be a disease in and of itself (Berger et al., 2013; Stumpf and Ständer, 2013). Unlike acute itch, which can facilitate removal of crawling insects, parasites, or irritants, persistent scratching in chronic itch disorders damages skin, leading to secondary infection, disfiguring lesions, and exacerbation of disease severity (Mack and Kim, 2018; Yosipovitch and Bernhard, 2013). One of the most common chronic itch disorders is atopic dermatitis (AD; commonly known as eczema), which affects fifteen million people in the US alone. Severe AD often leads to the atopic march, where chronic itch and inflammation progress to food allergy, allergic rhinitis, and asthma.

Little is known about the underlying mechanisms that drive chronic itch pathogenesis. As such, studies of human chronic itch disorders have sought to identify candidate mechanisms of disease progression. A number of studies have identified biomarkers and disease genes in human atopic dermatitis (AD) itch lesions (BS et al., 2012; Ewald et al., 2017; Guttman-Yassky et al., 2009; Jabbari et al., 2012; Li et al., 2014; Suárez-Fariñas et al., 2015). Indeed, a recent study compared the transcriptomes of healthy skin to itchy and non-itchy skin from psoriasis and AD patients, revealing dramatic changes in expression of genes associated with cytokines, immune cells, epithelial cells, and sensory neurons (Nattkemper et al., 2018). However, due to the difficulty in staging lesion development and obtaining staged samples from patients, there is currently no temporal map of when individual molecules and cell types contribute to chronic itch pathogenesis. Furthermore, the use of human patient data does not allow for rigorous mechanistic study of how disease genes contribute to chronic itch. To this end, we used a well-characterized inducible animal model of itch to define where, when, and how these genes identified from patient data contribute to chronic itch pathogenesis.

We employed the MC903 mouse model of AD and the atopic march (Dai et al., 2017; Li et al., 2009a; 2006; Moosbrugger-Martinz et al., 2017; Zhang et al., 2009) to provide a framework in which to identify the molecules and cells that initiate the development of atopic itch. The MC903 model is ideal for this approach because of its well-defined time course of lesion development and scratching onset (Li et al., 2006; Morita et al., 2015; Oetjen et al., 2017; Zhang et al., 2009). While MC903 has been widely used to study the chronic phase of AD (Kim et al., 2013; 2014; Li et al., 2006; 2009b; Naidoo et al., 2018; Oetjen et al., 2017; Zhang et al., 2009), we hypothesized that MC903 could also be used to define the early mechanisms underlying the

development of chronic itch, beginning with healthy skin. We performed RNA-seq of skin at key time points in the model and complemented this approach with measurements of itch behavior and immune cell infiltration. The primary goal of our study was to identify the inciting molecules and cell types driving development of chronic itch. To that end we found that infiltration of neutrophils into skin is required for development of chronic itch behaviors. Additionally, we demonstrate that early hyperinnervation of skin, and upregulation of itch signaling molecules and activity-induced genes in neurons are also dependent on neutrophils. Finally, we identify CXCL10/CXCR3 signaling as a key link between infiltrating neutrophils and sensory neurons that drives itch behaviors.

MC903 triggers rapid changes in expression of skin barrier, epithelial cell-derived cytokine, and axon guidance genes

Although a variety of AD- and chronic itch-associated genes have been identified, when and how they contribute to disease pathogenesis is unclear. Using RNA-seq of MC903-treated skin, we observed distinct temporal patterns by which these classes of genes were differentially expressed across the first eight days of the model (Figure 1A-B, Figure 1-Figure Supplement 1A). Proteases (*Klk6*, *Klk13*, among others) and skin barrier genes (*Cdhr1*) changed as early as six hours after the first treatment, before mice begin scratching (Figure 1A). Increased protease activity in AD skin is thought to promote breakdown of the epidermal barrier and release of inflammatory cytokines from keratinocytes (Steinhoff et al., 2003; Yosipovitch, 2004). One such cytokine, thymic stromal lymphopoetin (TSLP) is a key inducer of the Type 2 immune response, which is characteristic of human AD and the MC903 model, via signaling in $CD4^+$ T cells, basophils, and other immune cells (Briot et al., 2009; Demehri et al., 2009; Gao et al., 2010; Kim et al., 2013; Li et al., 2009a; Zhang et al., 2009). Beginning at day two, before any significant itch-evoked scratching (Figure 1A), immune cell infiltration (Figure 1E-G, Figure 1-Figure Supplement 2A-C), or skin lesions (data not shown) were observed, we saw increases in *Tslp*, as well as several other epithelial-derived cytokines, including the neutrophil chemoattractant genes *Cxcl1, Cxcl2, Cxcl3,* and *Cxcl5* (Figure 1D). To ask whether upregulation of these chemokine genes was dependent on protease activity, we treated human keratinocytes with the Protease Activated Receptor 2 agonist SLIGRL. SLIGRL treatment triggered increased expression of several of these chemokine genes, including *IL-8*, the human ortholog of mouse *Cxcl1/Cxcl2,* and *CXCL2* (Figure 1-Figure Supplement 3A). These increases occurred after a few hours of exposure to SLIGRL, suggesting that increased protease activity can rapidly trigger increases in neutrophil chemokines in skin, similar to what we observe in MC903-treated mouse skin.

Unexpectedly, we observed early changes in a number of transcripts encoding neuronal outgrowth factors (*Ngf*, *Artn*) and axon pathfinding molecules (*Slit1*, *Sema3d, Sema3a*), some of which are directly implicated in chronic itch (Hidaka et al., 2016; Kou et al., 2012; Tominaga et al., 2008; Tominaga and Takamori, 2014); Figure 1-Figure Supplement 4A), prior to when mice began scratching. We thus used immunohistochemistry (IHC) of whole-mount skin to examine skin innervation at this time point. We saw increased innervation of lesions at day two but not day one of the model (Figure 1H-I, Figure 1-Figure Supplement 5A). This increase came as a surprise because such changes had previously only been reported in mature lesions from human chronic itch patients (Haas et al., 2010; Kamo et al., 2013; Nattkemper et al., 2018; Oaklander and Siegel, 2005; Pereira et al., 2016; Schüttenhelm et al., 2015; Tominaga et al., 2009). Our findings suggest that early hyperinnervation is promoted by local signaling in the skin and is independent of the itch-scratch cycle.

Neutrophils are the first immune cells to infiltrate AD skin

At day five, mice exhibited robust itch behaviors and stark changes in a number of AD disease genes (Figure 1A-B). For example, loss-of-function mutations in filaggrin (*FLG)* are a major risk factor for human eczema (Palmer et al., 2006). Interestingly, *Flg2* levels sharply decreased by this time point. In parallel, we saw a continued and significant elevation in neutrophil and basophil chemoattractant genes (*Cxcl1,2,3,5*, and *Tslp*, Figure 1D). Using flow cytometry, we determined that neutrophils were the most highly increased cell type in the skin at day five (Figure 1E). It was not until day eight that we observed the classical AD-associated immune signature (Gittler et al., 2012) in the skin, with upregulation of *Il4, Il33* and other Th2-associated genes (Figure 1B, Figure 1D). We also observed increases in the T cell chemoattractants *Cxcl9, Cxcl10,* and *Cxcl11* (Figure 1D), which are thought to be hallmarks of chronic AD lesions in humans (Mansouri and Guttman-Yassky, 2015; Oetjen and Kim, 2018). Neutrophils and a number of other immune cells that started to infiltrate on day five were significantly elevated in skin by day eight, including basophils (Figure 1F), $CD4^+$ T cells (Figure 1G), inflammatory monocytes (Figure 1-Figure Supplement 2A), and mast cells (Figure 1-Figure Supplement 2B), but not eosinophils (Figure 1-Figure Supplement 2C).

$CD4^+$ T cells are ubiquitous in human AD lesions (Guttman-Yassky and Krueger, 2017) and have been shown to play a key role in promoting chronic AD itch and inflammation (Oetjen et al., 2017). More specifically, they are implicated in IL4Rα-dependent sensitization of pruriceptors in the second week of the MC903 model (Oetjen et al., 2017). Thus, we were quite surprised to find that itch behaviors preceded significant $CD4^+$ T cell infiltration. Therefore, neutrophils drew our attention as potential early mediators of MC903 itch. While neutrophil infiltration is a hallmark of acute inflammation, it remains unclear whether neutrophils contribute to the pathogenesis of chronic itch. Moreover, neutrophils release known pruritogens, including proteases and/or histamine, and secrete inflammatory lipids and cytokines that sensitize and/or activate pruriceptors (Dong and Dong, 2018; Hashimoto et al., 2018). Increased levels of PGE_2 and the neutrophil-specific lipid LTB_4 have also been reported in skin of AD patients (Fogh et al., 1989). Indeed, by mass spectrometry, we observed increases in several of these inflammatory lipids, PGD_2 and PGE_2, as well as LTB_4 and its precursor 5-HETE (Figure 1-Figure Supplement 6A). Thus, we next tested the requirement of neutrophils to itch in the MC903 model.

Neutrophils are required for early itch behaviors in the MC903 model of AD

We first asked whether neutrophils were required for MC903-evoked itch by depleting neutrophils, the earliest and largest population of infiltrating immune cells in this chronic itch model. Depletion of neutrophils by daily injections of an anti-Gr1 (aGr1) antibody (Ghasemlou et al., 2015; Kim et al., 2009; Sivick et al., 2014) dramatically attenuated itch-evoked scratching through the first eight days of the model (Figure 2A). Consistent with a key role for neutrophils in driving chronic itch, our depletion strategy significantly and selectively reduced circulating and skin infiltrating neutrophils on days five and eight, days on which control, but not depleted mice, scratched robustly (Figure 2B; Figure Supplement 1A-C). In contrast, basophils and $CD4^+$ T cells continued to infiltrate the skin following aGr1 treatment (Figure 2C-D), suggesting that these cells are not required for early MC903 itch.

We next used the cheek model of acute itch (Shimada and LaMotte, 2008) to ask whether neutrophil recruitment is sufficient to trigger itch. As expected, we observed significant and selective recruitment of neutrophils to cheek skin within 15 minutes after CXCL1 injection (Figure 2-Figure Supplement 2A-B). CXCL1 injection also triggered robust scratching behaviors (Figure 2E) on a similar time course to neutrophil infiltration (Figure 2 - Figure Supplement 2B). Thus, we depleted neutrophils with aGr1 to determine whether neutrophils were required for CXCL1-evoked acute itch. Indeed, aGr1-treatment significantly reduced numbers of skin-

infiltrating neutrophils (Figure 2-Figure Supplement 3A) and resulted in a dramatic loss of CXCL1-evoked itch behaviors (Figure 2C). This effect was specific to neutrophil-induced itch as injection of chloroquine, a pruritogen that directly activates sensory neurons, triggered robust scratching in aGr1-treated animals (Figure 2-Figure Supplement 4A). Given that CXCL1 has been shown to directly excite and/or sensitize sensory neurons (Deftu 2017,2018), it is possible that the CXCL1 mechanism in itch may also involve neuronal pathways. However, our results show that CXCL1-mediated neutrophil infiltration is sufficient to drive acute itch behaviors, and that neutrophils are necessary for itch in the MC903 model.

We also examined the MC903-evoked itch behaviors of mice deficient in *Crlf2*, the gene encoding the TSLP receptor (TSLPR$^{-/-}$ mice; (Carpino et al., 2004). TSLPR is expressed by both immune cells and sensory neurons and is a key mediator of atopic dermatitis in human and mouse models. Surprisingly, MC903-treated TSLPR$^{-/-}$ mice displayed robust scratching behaviors during the first eight days of the model (Figure 2F). In contrast to our results in aGR1-injected mice, TSLPR$^{-/-}$ mice displayed robust neutrophil infiltration (Figure 2G), but a complete loss of basophil and CD4^{+} T cell infiltration into the skin (Figure 2H-I). These results suggest that basophils and T cells are not required for early itch and further support an inciting role for neutrophils. Previous studies have shown that TSLP drives the expression of Type 2 cytokines and related immune cells that promote itch and inflammation in mature AD skin lesions and in the second week of the MC903 AD model (Briot et al., 2009; Demehri et al., 2009; Li et al., 2009a; Zhang et al., 2009). Consistent with a later stage role for TSLP signaling in AD, we did observe a significant reduction in itch-evoked scratching in TSLPR$^{-/-}$ mice in the second week of the model (Figure 2F). Thus, our data support a model in which neutrophils are necessary for initiation of AD and itch behaviors early in the development of AD, while TSLPR signaling mediates the recruitment of basophils and CD4^{+} T cells to promote later stage itch and chronic inflammation.

MC903 drives rapid and robust changes in the peripheral and central nervous systems

But how do neutrophils drive MC903 itch? Itchy stimuli are detected and transduced by specialized subsets of peripheral somatosensory neurons. Thus, to answer this question we first profiled the transcriptional changes in somatosensory neurons in the MC903 model, which were previously unstudied. In general, little is known regarding neuronal changes in chronic itch. Our initial examination of early hyperinnervation and changes in axon guidance molecules in skin suggested that neurons are indeed affected early on in the MC903 model, before the onset of itch-evoked scratching behaviors. In contrast to the skin, where we saw many early transcriptional changes, we did not see any significant transcriptional changes in the trigeminal ganglia (TG) until five days after the first treatment, and in total only 84 genes were differentially expressed through the eighth day (Figure 3A-B). These hits included genes related to excitability of itch sensory neurons (Dong and Dong, 2018; Usoskin et al., 2015), neuroinflammatory genes (Takeda et al., 2009) and activity-induced or immediate early genes (Figure 3A). Interestingly, we observed enrichment of neuronal markers expressed by one specific subset of somatosensory neurons that are dedicated to itch (*Il31ra, Osmr, Trpa1, Cysltr2,* and *Nppb* (Solinski et al., 2019; Usoskin et al., 2015), termed “NP3” neurons. Similar to what has been reported in mouse models of chronic pain, we observed changes in neuroinflammatory (*Bdnf, Nptx1, Nptx2, Nptxr*) and immune genes (*Itk, Cd19, Rag, Tmem173*). However, these transcriptional changes occurred just a few days after itch onset, in contrast to the slow changes in nerve injury and pain models that occur over weeks (Scholz and Woolf, 2007), indicating that neuropathic changes may occur sooner than previously thought. These changes occurred in tandem with the onset of scratching behaviors (Figure 1C), suggesting that the early molecular and cellular changes we observed by this time point may be important for development of itch-evoked scratching.

The changes we observed in immune-related genes in the TG were suggestive of infiltration or expansion of immune cell populations, which has been reported in models of nerve injury and chronic pain, but has never been reported in chronic itch. To validate our observations, we used IHC to ask whether $CD45^+$ immune cells increase in the TG. We observed a significant increase in immune cell counts at day eight but not day five (Figure 3C-F, Figure 3-Figure Supplement 1A-D). Because we observed such dramatic expression changes in the TG on day eight of the model, we postulated that the CNS may also be affected at this time point. Thus, we performed RNA-seq on spinal cord segments that innervate the rostral back skin of MC903-treated mice. To date, only one study has examined changes in the spinal cord during chronic itch. They showed that upregulation of the STAT3-dependent gene *Lcn2* occurred three weeks after induction of chronic itch and was essential for sustained scratching behaviors (Shiratori-Hayashi et al., 2015). Surprisingly, we saw upregulation of *Lcn2* on day eight of the MC903 model and, additionally, we observed robust upregulation of immediate early genes (*Fos, Junb,* Figure 3G), suggesting that MC903 itch drives activity-dependent changes in the spinal cord as early as one week after beginning treatment. Together our findings show that sustained itch and inflammation can drive changes in the PNS and CNS much sooner than previously thought, within days rather than weeks after the onset of scratching. We next set out to ask how loss of neutrophils impacted the molecular changes observed in skin and sensory neurons in the MC903 model, and which of these changes might contribute to neutrophil-dependent itch.

Neutrophils are required for upregulation of select itch- and atopic-related genes, including the itch-inducing chemokine CXCL10

To ask how neutrophils might promote itch in the MC903 model, we examined the transcriptional changes in skin and sensory ganglia isolated from non-itchy neutrophil-depleted animals and from the $TSLPR^{-/-}$ mice, which scratched robustly. In both the neutrophil-depleted and $TSLPR^{-/-}$ skin, several AD-associated cytokines were similarly dysregulated, including *Il33* (Figure 4A, Figure 4-Figure Supplement 1A). Expression of epithelial-derived cytokines and chemokines *Tslp*, *Cxcl1*, *Cxcl2*, *Cxcl3*, and *Cxcl5* were unaffected by either loss of TSLPR or neutrophil depletion (Figure 4B), suggesting these molecules are produced by skin cells even when the MC903-evoked immune response is compromised. Among the hundreds of MC903-dependent genes we examined, only a handful of genes were uniquely affected by aGr1 treatment. One such gene was *Cxcl10*, a chemokine known to be released by skin epithelial cells, neutrophils, and other myeloid cells (Hashimoto et al., 2018; Ioannidis et al., 2016; Kanda et al., 2007; Koga et al., 2008; Michalec et al., 2002; Padovan et al., 2002; Tamassia et al., 2007). *Cxcl10* expression was increased in $TSLPR^{-/-}$ but not neutrophil-depleted skin (Figure 4B, Figure 4-Figure Supplement 1A). CXCL10 has been previously shown to drive acute itch in a model of allergic contact dermatitis via CXCR3 signaling in sensory neurons (Qu et al., 2015), and is elevated in skin of AD patients (Mansouri and Guttman-Yassky, 2015). Expression of *Cxcl9* and *Cxcl11*, two other CXCR3 ligands that are elevated in AD but have an unknown role in itch, was also decreased in AD skin of neutrophil-depleted mice (Figure 4B).

CXCR3 signaling is necessary for MC903-evoked chronic itch

We hypothesized that neutrophil-dependent upregulation of CXCL10 activates sensory neurons to drive itch behaviors. Consistent with this model, neutrophil depletion attenuated the expression of activity-induced immediate early genes (*Vgf, Junb*) in the TG, suggestive of neutrophil-dependent sensory neuronal activity in the MC903 model (Figure 4C, Figure 4-Figure Supplement 1B). We found that neutrophils also contributed to other sensory neuronal phenotypes in the model. For example, we observed that expression of *Lcn2*, a marker of neuropathic itch, and activity-induced genes *Fos* and *Junb* were not increased in spinal cord isolated from neutrophil-depleted animals after MC903 treatment, indicating that neutrophil-

dependent scratching behaviors may indeed drive changes in the CNS (Figure 4D). We also observed that neutrophil-depleted animals displayed no skin hyperinnervation at day two (Figure 4E). This result was surprising because we did not observe significant neutrophil infiltration at this early time point, but these data suggest that low numbers of neutrophils are sufficient to mediate these early effects.

To test our model wherein CXCL10 activation of CXCR3 drives neutrophil-dependent itch, we first asked whether this CXCR3 ligand is in fact released in MC903-treated skin. We performed ELISA on cheek skin homogenate and found that CXCL10 protein was increased in MC903-treated skin, but not in skin from neutrophil-depleted mice (Figure 4F). To test whether CXCR3 signaling directly contributes to MC903-evoked itch, we asked whether acute blockade of CXCR3 signaling using the antagonist AMG 487 (Qu et al., 2015) affected scratching behaviors in the MC903 model. We found that the CXCR3 antagonist strongly attenuated scratching behaviors on days five, eight, and twelve (Figure 4G), with the greatest effect at day eight. In contrast, CXCR3 blockade did not attenuate scratching behaviors in naive mice injected with the pruritogen chloroquine (Figure 4G), demonstrating that CXCR3 signaling contributes to chronic itch but is not required for scratching in response to acute pruritogens. Thus, we propose that neutrophils promote chronic itch via upregulation of CXCL10 and subsequent activation of CXCR3 (Figure 5).

Discussion

There is great interest in unraveling the neuroimmune interactions that promote acute and chronic itch. Here, we show that neutrophils are essential for the early development of MC903-evoked itch. We further show that the acute recruitment of neutrophils to the skin is sufficient to drive itch behaviors within minutes of infiltration. While neutrophils are known to release a variety of pruritogens, their roles in itch and AD were not studied (Hashimoto et al., 2018). Only a few studies have even reported the presence of neutrophils in human AD lesions (BS et al., 2012; Koro et al., 1999; Mihm et al., 1976; Shalit et al., 1987). Neutrophils have been implicated in psoriatic inflammation and inflammatory pain (Carreira et al., 2013; Cunha et al., 2008; Pinho-Ribeiro et al., 2018; Sumida et al., 2014), where they are thought to rapidly respond to tissue injury and inflammation (Kim and Luster, 2015; Kolaczkowska and Kubes, 2013), but they have not been directly linked to itch. A previous study showed that the neutrophil chemoattractant *Cxcl1* was elevated in a mouse model of dry skin itch (Wilson et al., 2013a). While tissue damage can trigger upregulation of neutrophil chemoattractants and neutrophil infiltration, *Cxcl1* expression was upregulated both in scratched and unscratched itchy skin, suggesting that upregulation of CXCL1, and subsequent neutrophil infiltration, is not simply a consequence of tissue damage or the itch-scratch cycle.

TSLP signaling triggers development of a Type 2 immune response, which is crucial for the progression of atopic disease. For example, Th2 cytokines, most notably IL-4 and IL-13, are thought to drive the transition from the acute to chronic phase of human AD, and IL4Rα signaling was recently shown to mediate inflammation and itch in the second week of the MC903 AD mouse model (Oetjen et al., 2017). Interestingly, the same study showed that IL-4 sensitizes the population of itch sensory neurons that responds to TSLP. Based upon their observation, and because TSLP is induced early on in the MC903 model, we expected TSLP to contribute to early MC903 itch. We were surprised to find that TSLPR signaling is dispensable for itch behaviors in the first week of the model, and is only required for itch in the second week. In light of our observation that neutrophils are required for early MC903 itch, and that TSLPR signaling is necessary for increased IL-4 production, we hypothesize that TSLPR signaling plays a key role in later, IL-4-dependent itch, whereas early itch is independent of IL-4. Our findings align well with a recent study showing that TSLP and IL4 act on overlapping sensory neuron

populations and that neuronal IL4Rα promotes itch during the second week of the MC903 model (Oetjen et al., 2017).

Given the large magnitude of the itch deficit in the neutrophil-depleted mice, we were surprised to find fewer expression differences in MC903-dependent, AD-associated genes between neutrophil depleted and non-depleted mice than were observed between WT and TSLPR$^{-/-}$ mice. One of the few exceptions were the Th1-associated genes *Cxcl9/10/11* (Brunner et al., 2017; Ewald et al., 2017). We found that induction of these genes and CXCL10 protein was completely dependent on neutrophils. While our results do not identify the particular cell type(s) responsible for neutrophil-dependent CXCL10 production, a number of cell types present in skin have been shown to produce CXCL10, including epithelial keratinocytes, myeloid cells, and sensory neurons (Flier et al., 2001; Hashimoto et al., 2018; Ioannidis et al., 2016; Kanda et al., 2007; Koga et al., 2008; Michalec et al., 2002; Padovan et al., 2002; Steain et al., 2011; Tamassia et al., 2007). We also observed striking differences in neutrophil-dependent gene expression in the spinal cord, where expression of activity-induced genes and the chronic itch gene *Lcn2* were markedly attenuated by loss of neutrophils. Our observations newly implicate neutrophils in setting the stage for the acute-to-chronic itch transition by triggering molecular changes necessary to develop a chronic, itchy lesion.

Additionally, we demonstrate a novel role of CXCR3 signaling in MC903-induced itch. The CXCR3 ligand CXCL10 contributes to mouse models of acute and allergic itch (Liu et al., 2016; Qu et al., 2015); however, its role in chronic itch was previously unknown. Our results show that CXCL10 upregulation is dependent on neutrophils and that CXCR3 blockade dramatically attenuates itch behaviors. Our findings are in alignment with a recent study showing that dupilumab, a new AD drug that blocks IL4Rα, a major downstream effector of the TSLP signaling pathway, does not significantly reduce CXCL10 levels in human AD lesions (Hamilton et al., 2014). Taken together, this suggests that the TSLP-IL-4 and neutrophil-CXCL10 pathways are not highly interdependent, and supports our findings that *Il4* is robustly upregulated in the absence of neutrophils. Additionally, targeting IL4Rα has been successful in treating itch and inflammation in some, but not all, AD patients (Simpson et al., 2016). We propose that biologics or compounds targeting neutrophils and/or the CXCR3 pathway may be useful for AD that is incompletely cleared by dupilumab monotherapy. Drugs targeting neutrophils are currently in clinical trials for the treatment of psoriasis, asthma, and other inflammatory disorders. For example, MDX-1100, a biologic that targets CXCL10, has already shown efficacy for treatment of rheumatoid arthritis in phase II clinical trials (Yellin et al., 2012). While rheumatoid arthritis and AD have distinct etiologies (Scott et al., 2010), our work indicates that CXCL10 or CXCR3 may be promising targets for treating chronic itch. Our findings may be applicable to other itch disorders such as psoriasis and ACD where neutrophil chemoattractants and/or CXCL10 are also elevated. Overall, our data suggest that neutrophils incite early itch and inflammation in the development of AD through several mechanisms, including: 1) directly triggering itch upon infiltration into the skin (e.g. by release of known sensitizing/itchy lipids such as PGE_2 and LTB_4, Figure 4) and, 2) indirectly triggering itch by altering expression of known pruritogens (e.g. induction of *Cxcl10* expression; (Flier et al., 2001; Hashimoto et al., 2018; Ioannidis et al., 2016; Kanda et al., 2007; Koga et al., 2008; Michalec et al., 2002; Padovan et al., 2002; Tamassia et al., 2007). These direct and indirect mechanisms for neutrophil-dependent itch may explain why neutrophils have a dramatic effect on scratching behaviors on not only day eight but also day five of the model, when neutrophils are recruited in large numbers, but CXCR3 ligands are not as robustly induced.

More generally, our study provides a framework for understanding how and when known human disease genes contribute to the distinct stages of chronic itch pathogenesis. Our analysis of

MC903-evoked transcriptional changes suggests we may be able to extend findings in the model not only to atopic dermatitis, but also to related disorders, including specific genetic forms of atopy. For example, we provide evidence that the MC903 model may also model the filaggrin loss-of-function mutations, which are a key inciting factor in human heritable atopic disease (Palmer et al., 2006; Schuttelaar et al., 2009). There are many rich datasets looking at mature patient lesions (BS et al., 2012; Ewald et al., 2017; Guttman-Yassky et al., 2009; Jabbari et al., 2012; Li et al., 2014; Suárez-Fariñas et al., 2015) and datasets for mature lesions in other mouse models of chronic itch (Liu et al., 2016; Oetjen et al., 2017; Swindell et al., 2011; 2017). Our study adds a temporal frame of reference to these existing datasets to probe the function of human disease genes in AD in greater detail. Furthermore, we have mapped the time course of gene expression changes in primary sensory ganglia and spinal cord during chronic itch development. We show that the MC903 model recapitulates several hallmarks of neuropathic disease on a time course much shorter than has been reported for chronic itch, or chronic pain. Nervous system tissues are extremely difficult to obtain from human AD patients, and thus little is known regarding the neuronal changes in chronic itch disorders in both mouse models and human patients. Our findings can now be compared to existing and future datasets examining neuronal changes in chronic pain, diabetic neuropathy, shingles, neuropathic itch, psoriasis, and other inflammatory disorders where neuronal changes are poorly understood but clearly contribute to disease progression. The early changes we see in skin innervation, sensory ganglia, and spinal cord dovetail nicely with recent studies examining neuroimmune interactions in other inflammatory conditions (Baral et al., 2018; Blake et al., 2018; Pinho-Ribeiro et al., 2018), which all implicate early involvement of sensory neurons in the pathogenesis of inflammatory diseases.

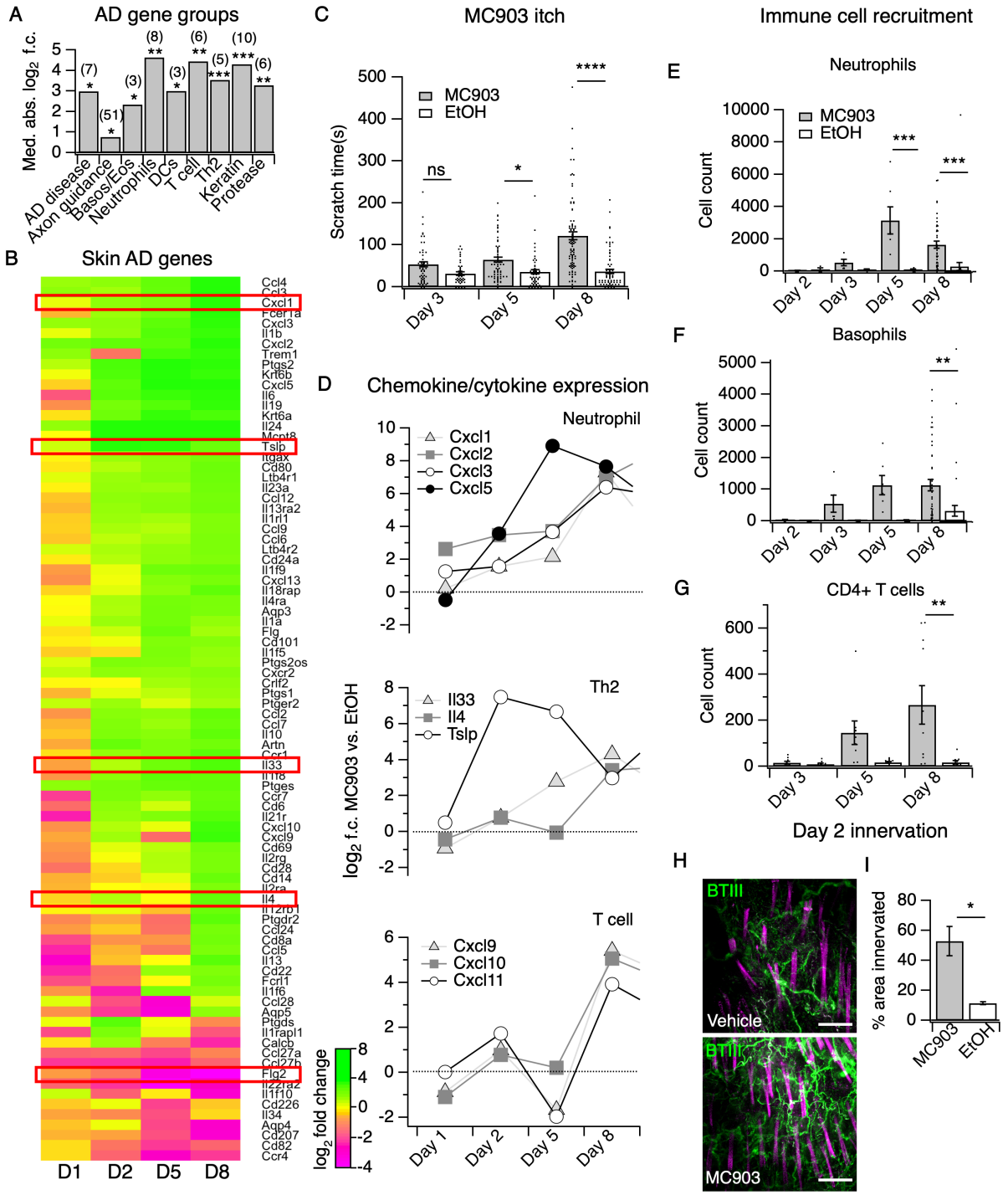

Figure 1

Figure 1. The MC903 model parallels the progression of human atopic disease and suggests a temporal sequence of AD pathogenesis. **A.** Exact permutation test (10,000 iterations, see Methods) for significance of mean absolute $\log_2$ fold change in gene expression at Day 8 (MC903 vs. ethanol) of custom-defined groups of genes for indicated categories (see **Figure 1-source data table 1**). **B.** Log_2 fold change in gene expression (MC903 vs. ethanol) in mouse skin at indicated time points for key immune and mouse/human atopic dermatitis genes that were significantly differentially expressed for at least one time point in the MC903 model.

Only genes from our initial list (see Methods) differentially expressed at corrected $p < 0.05$ and changing > 2-fold between treatments for at least one condition are shown. Green bars = increased expression in MC903 relative to ethanol; magenta = decreased expression. Exact values and corrected *p*-values are reported in **Figure 1-source data table 2** and **Supplemental Data**, respectively. D1 = 6 hours post-treatment; D2 = Day 2; D5 = Day 5; D8 = Day 8. **C.** Scratching behavior of mice treated with MC903 or ethanol for indicated length of time (two-way ANOVA: ****$p_{\text{interaction}} < 0.0001$, F(2,409) = 13.25; Sidak's multiple comparisons: $p_{day\ 3} = 0.1309$, n=62,51 mice; *$p_{day\ 5} = 0.0171$, n=69,56 mice; ****$p_{day\ 8} < 0.0001$, n=92,85 mice). Exact values displayed in **Figure 1-source data table 3**. **D.** Log_2 fold change in gene expression of neutrophil chemoattractants (upper), Th2 cytokines (middle) and T cell chemoattractants (lower, from RNA-seq data). **E.** Neutrophil counts in MC903- and ethanol-treated skin at indicated time points (two-way ANOVA: **$p_{\text{treatment}} = 0.0023$, F(1,102) = 9.82; Sidak's multiple comparisons: $p_{day\ 2} > 0.999$, n=4,4 mice; $p_{day\ 3} = 0.9801$, n=5,5 mice; ***$p_{day\ 5} = 0.0003$, n=6,8 mice; ***$p_{day\ 8} = 0.0001$, n=40,38 mice). **F.** Basophil counts in MC903- and ethanol-treated skin at indicated time points (two-way ANOVA: *$p_{\text{treatment}} = 0.0215$, F(1,102) = 5.45; Sidak's multiple comparisons: $p_{day\ 2} > 0.999$, n=4,4 mice; $p_{day\ 3} = 0.8566$, n=5,5 mice; $p_{day\ 5} = 0.1280$, n=6,8 mice; **$p_{day\ 8} = 0.0010$, n=40,38 mice). **G.** $CD4^+$ T cell counts in MC903- and ethanol-treated skin at indicated time points (two-way ANOVA: **$p_{\text{time}} = 0.0042$, F(1,44) = 9.10; $p_{day\ 3} = 0.9998$, n=8,6 mice; $p_{day\ 5} = 0.2223$, n=9,8 mice; **$p_{day\ 8} = 0.0021$, n=11,8 mice). Exact values displayed in **Figure 1-source data table 4**. **H.** Representative maximum intensity Z-projections from immunohistochemistry (IHC) of whole-mount mouse skin on Day 2 of the MC903 model. Skin was stained with neuronal marker beta-tubulin III (BTIII; green). Hair follicle autofluorescence is visible in the magenta channel. Images were acquired on a confocal using a 20x water objective. **I.** Quantification of innervation (see Methods) of mouse skin as determined from BTIII staining (*p = 0.012; two-tailed t-test (t =3.114; df =9); n = 7,4 images each from 2 mice per treatment). Day 1 IHC results as follows: 31.78 ± 18.39 % (MC903) and 31.51 ± 16.43 % (EtOH); p = 0.988; two-tailed unpaired t-test; n = 6 images each from 2 mice per treatment. Exact values are reported in **Figure 1-source data table 5**.

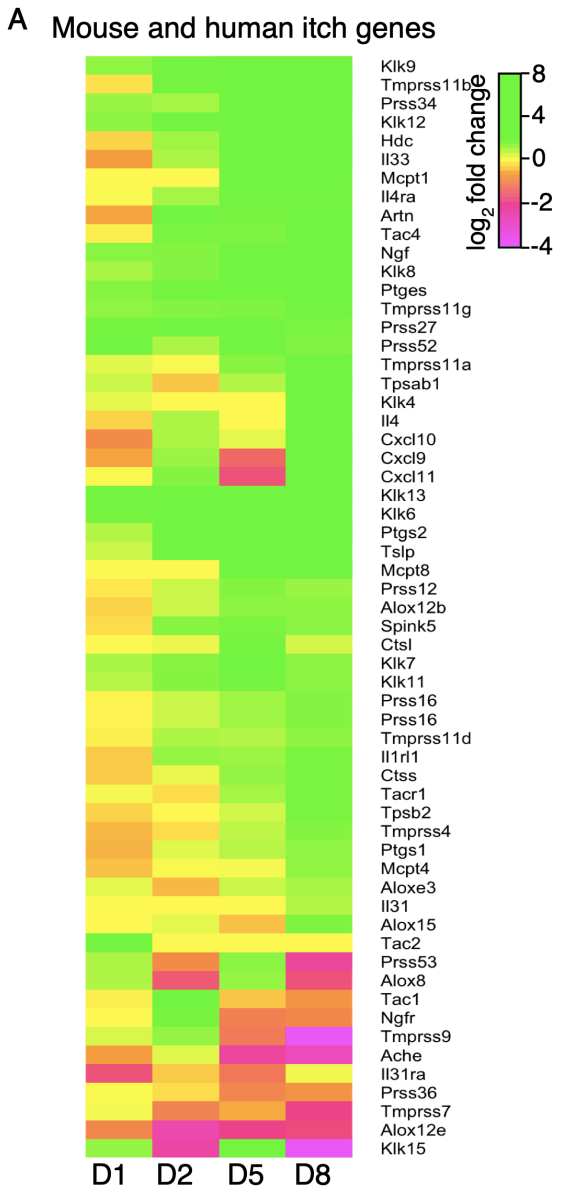

Figure 1-Figure Supplement 1

Figure 1-Figure Supplement 1. Expression of mouse and human itch genes. A. Log_2 fold change in gene expression (MC903 vs. ethanol) in mouse skin at indicated time points for genes implicated in mouse or human acute or chronic itch that were significantly differentially expressed for at least one time point in the MC903 model. Green bars = increased expression in MC903 relative to ethanol; magenta = decreased expression. Exact values and corrected *p*-values are reported in **Figure 1-source data table 6** and **Supplemental Data**, respectively.

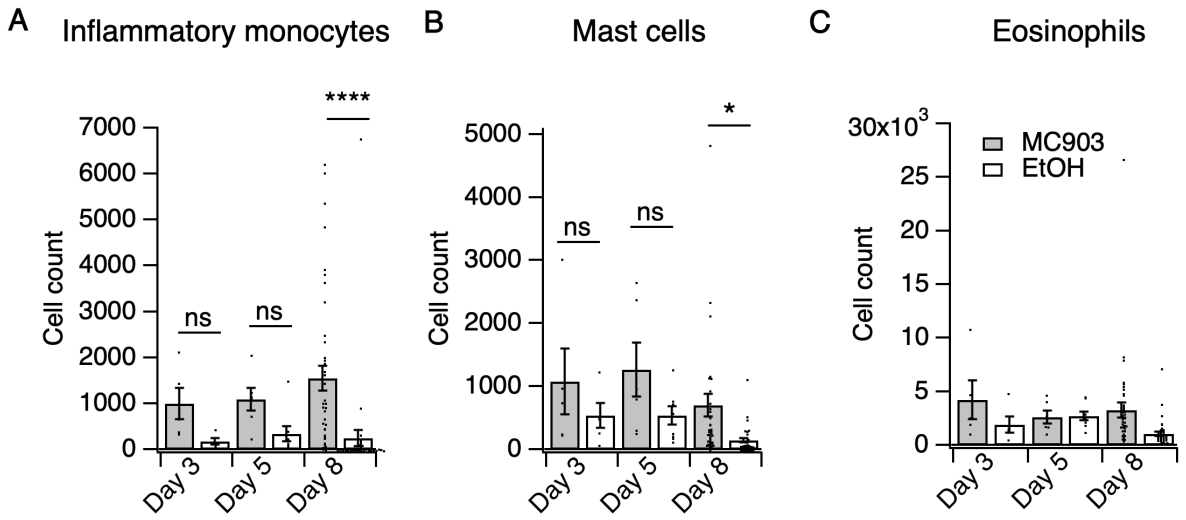

Figure 1-Figure Supplement 2

Figure 1-Figure Supplement 2. Immune cell counts in MC903-treated skin. A. Inflammatory monocyte counts in MC903- and ethanol-treated skin at indicated time points (two-way ANOVA: *$p_{treatment}$= 0.0129, F(1,96) = 6.42; Sidak's multiple comparisons: $p_{day\ 3}$ = 0.6933, n=5,5 mice; $p_{day\ 5}$ = 0.6536, n=6,8 mice; ****$p_{day\ 8}$ < 0.0001, n=40,38 mice). **B.** Mast cell counts in MC903- and ethanol-treated skin at indicated time points (two-way ANOVA: *$p_{treatment}$= 0.0117, F(1,96) = 6.60; Sidak's multiple comparisons: $p_{day\ 3}$ = 0.6562, n=5,5 mice; $p_{day\ 5}$ = 0.2829, n=6,8 mice; *$p_{day\ 8}$ = 0.0115, n=40,38 mice). Data from mice receiving i.p. injection of PBS (see Figure 4) in addition to MC903 or EtOH are also included. **C.** Eosinophil counts in MC903- and ethanol-treated skin at indicated time points (two-way ANOVA: $p_{treatment}$= 0.0964, F(1,96) = 2.81, n=4,5,5,8,38,38 mice). Exact values displayed in **Figure 1-source data table 4**.

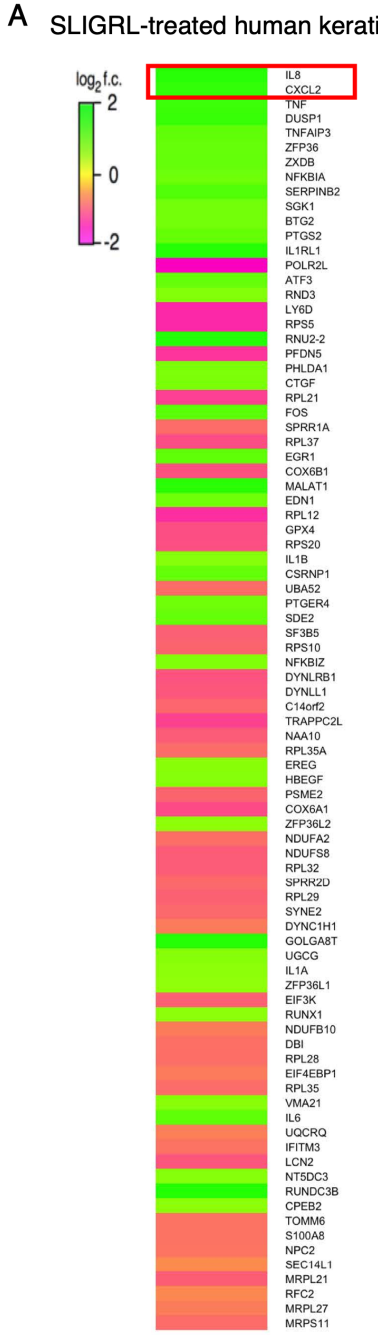

Figure 1-Figure Supplement 3

Figure 1-Figure Supplement 3. Protease receptor activation triggers rapid upregulation of neutrophil chemokine genes in human keratinocytes. A. Heat map showing $\log_2$ fold change in gene expression in cultured human keratinocytes 3 hours after SLIGRL treatment (100 μM; bottom; see **Figure 1-source data table 7**) compared to vehicle controls, as measured by RNA-seq. Genes are sorted by descending corrected *p*-value; only significantly differentially expressed ($p < 0.05$) are displayed. Exact values and corrected *p*-values are reported in **Figure 1-source data table 7** and **Supplemental Data**, respectively.

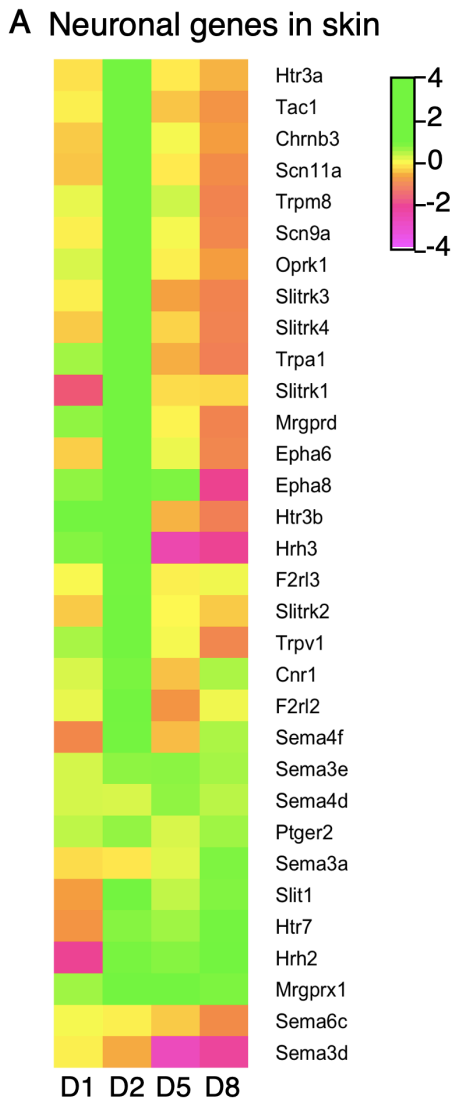

Figure 1-Figure Supplement 4

Figure 1-Figure Supplement 4. Expression of neuronal genes and axon guidance molecules in skin. A. Log_2 fold change in gene expression (MC903 vs. EtOH) in mouse skin at indicated time points for markers of locally translated sensory neuronal transcripts or genes implicated in neurite remodeling and/or axon guidance that were significantly differentially expressed for at least one time point in the MC903 model. Green bars = increased expression in MC903 relative to ethanol; magenta = decreased expression. Exact values and corrected *p*-values are reported in **Figure 1-source data table 7** and **Supplemental Data**, respectively.

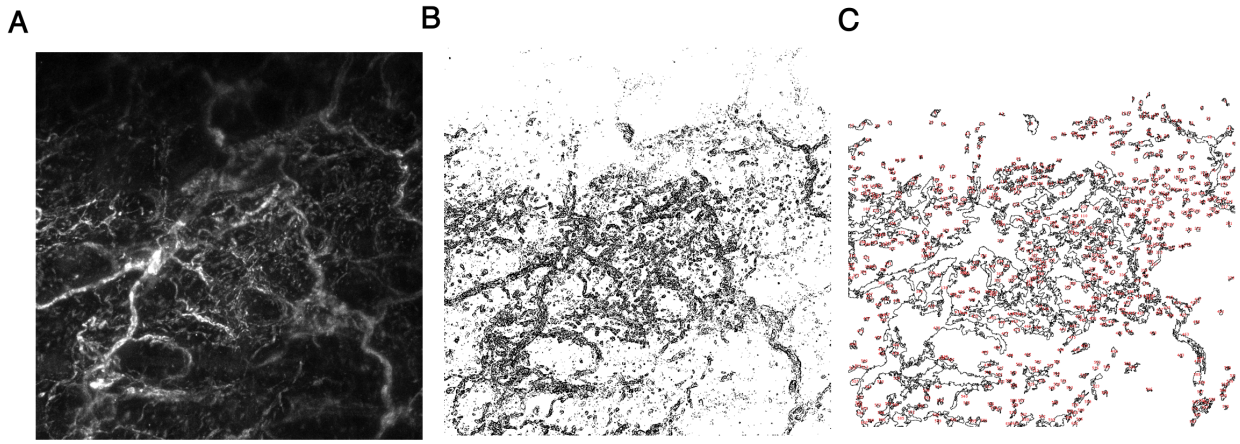

Figure 1-Figure Supplement 5

Figure 1-Figure Supplement 5. Method of image quantification for whole mount skin. **A.** Representative maximum intensity z-projection of beta tubulin III staining in cheek skin. **B.** Binary image after edge-detection. **C.** % Area innervated was calculated from the percentage of the image area which was occupied by the regions of interest (ROIs) outlined in red.

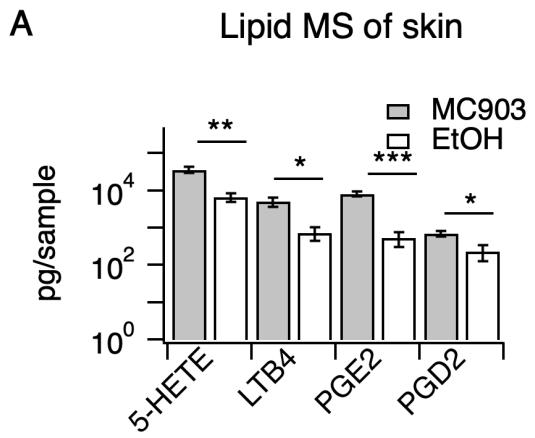

Figure 1-Figure Supplement 6

Figure 1-Figure Supplement 6. Inflammatory lipids in MC903-treated skin. A. Quantification of indicated lipids from 6 mm biopsy punches of cheek skin of MC903- and EtOH-treated mice (at day 8) by LC-MS/MS (**p = 0.006 (*t*=4.148,*df*=6), *p = 0.024 (*t*=3.003,*df*=6), ***p = 0.0007 (*t*=6.392,*df*=6), *p = 0.022 (*t*=3.058,*df*=6); two-tailed unpaired t-tests; n = 4 mice per group, see **Figure 1-source data table 8**).

Figure 1-source data table 1. Values displayed in the bar plot shown in Figure 1A.
Figure 1-source data table 2. Values displayed in the heat map shown in Figure 1B.
Figure 1-source data table 3. Values displayed in the bar plot shown in Figure 1C.
Figure 1-source data table 4. Values displayed in the bar plots shown in Figure 1E-G and Figure 1-Figure Supplement 2A-C.
Figure 1-source data table 5. Values displayed in the bar plot shown in Figure1I.
Figure 1-source data table 6. Values displayed in the heat map shown in Figure1-Figure Supplement 1A.
Figure 1-source data table 7. Values displayed in the heat map shown in Figure1-Figure Supplement 3A.
Figure 1-source data table 8. Values displayed in the heat map shown in Figure1-Figure Supplement 4A.
Figure 1-source data table 9. Values displayed in the bar plot shown in Figure1-Figure Supplement 6A.

Supplementary Table 1. Number of mapped reads and sample information for all RNA-seq samples represented in the manuscript.

Supplementary Table 2. Outputs of statistical tests performed on behavioral and flow cytometry data to determine whether select data sets could be combined.

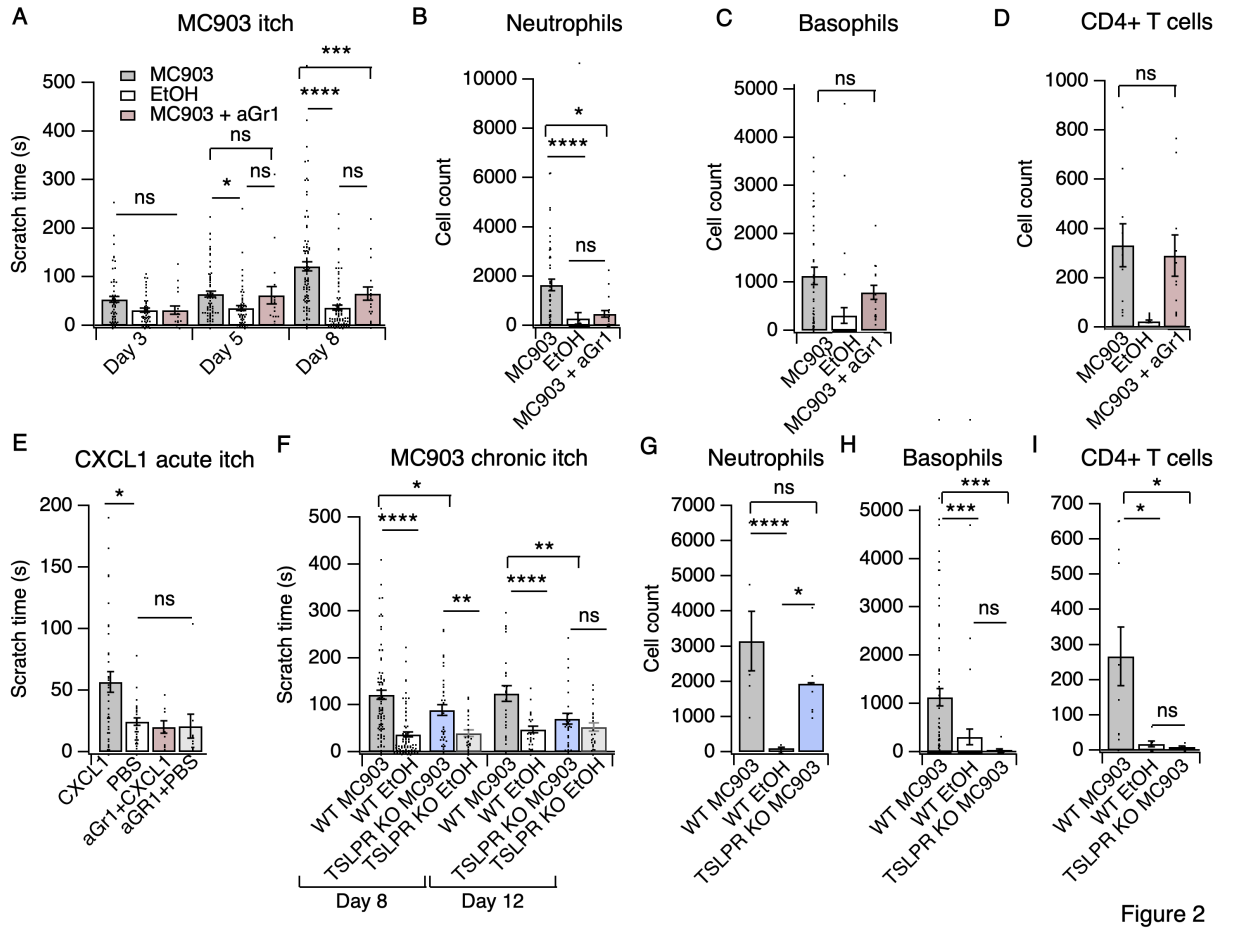

Figure 2

Figure 2. Neutrophils are necessary and sufficient for itch behaviors. A. Scratching behavior of uninjected and PBS-injected mice (combined) and aGr1-injected mice treated with MC903 or ethanol for indicated length of time (two-way ANOVA: ****$p_{\text{interaction}} < 0.0001$, F(4,447) = 7.16; Tukey's multiple comparisons: $p_{day\ 3} > 0.05$, n=62,51,17 mice; *$p_{day\ 5} = 0.0154$, $p_{day\ 5} = 0.9854$, $p_{day\ 5} = 0.2267$, n=69,56,17 mice; ****$p_{day\ 8} < 0.0001$, ***$p_{day\ 8} = 0.0007$, $p_{day\ 8} = 0.1543$, n=92,85,17 mice). **B.** Neutrophil count from cheek skin of uninjected/PBS-injected MC903- and ethanol-treated, and aGr1-injected MC903-treated mice on day 8 (one-way ANOVA: ****$p < 0.0001$, F(2,92) = 10.59; Tukey's multiple comparisons: ****$p_{MC903\ vs.\ EtOH} < 0.00001$, n=40,38 mice; $p_{MC903\ vs.\ aGr1\ MC903} = 0.0109$, n=40,17 mice). **C.** Basophil count from cheek skin of uninjected/PBS-injected MC903- and ethanol-treated, and aGr1-injected MC903-treated mice on day 8 (one-way ANOVA: **$p = 0.0025$, F(2,92) = 6.397; Tukey's multiple comparisons: $p_{MC903\ vs.\ aGr1\ MC903} = 0.4848$, n=40,17 mice). **D.** $CD4^+$ T cell count from cheek skin of uninjected/PBS-injected MC903- and ethanol-treated, and aGr1-injected MC903-treated mice on day 8 (two-way ANOVA: *$p_{treatment} = 0.0286$, F(1,26) = 5.373; Holm-Sidak multiple comparisons for PBS versus aGr1: $p_{MC903} = 0.8127$, n=8,10 mice; $p_{EtOH} = 0.7131$, n=6,6 mice). Control MC903 and EtOH data from **Figure 2B-C** are also displayed in **Figure 1**. Exact values displayed for **Figure 2A-D** in **Figure 2-source data table 1**. **E.** Scratching behavior of mice immediately after injection of 1 µg CXCL1 or PBS (i.d. cheek). For neutrophil-depletion experiments, mice received 250 µg anti-Gr1 (aGr1) 20 hours prior to cheek injection of CXCL1 or PBS (one-way ANOVA: ****$p < 0.0001$, F(4,88) = 75.53; Tukey's multiple comparisons: *$p_{CXCL1\ vs.\ PBS} = 0.0126$, n=36,31 mice; $p_{aGr1\text{-}CXCL1\ vs.\ aGr1\text{-}PBS} > 0.9999$, n=10,10 mice; $p_{aGr1\text{-}CXCL1\ \text{vs. PBS}} = 0.9986$, n=10,31 mice). Exact values displayed in **Figure 2-source data table 2**. **F.** Scratching behavior of WT and $TSLPR^{-/-}$ (TSLPR KO) mice treated with MC903 or ethanol for indicated length of time (two-way ANOVA:

507 ****$p_{\text{interaction}}$ < 0.0001, F(9,657) = 4.93; Tukey's multiple comparisons: ****$p_{day\ 8}$ < 0.0001, *$p_{day\ 8}$
508 = 0.0194, **$p_{day\ 8}$ = 0.0039, n=92,85,36,26 mice; ****$p_{day\ 12}$ < 0.0001, **$p_{day\ 12}$ = 0.0028, $p_{day\ 12}$ =
509 0.7061, n=26,26,27,23 mice). **G.** Neutrophil count from cheek skin of wild-type MC903- and
510 ethanol-treated, and TSLPR$^{-/-}$ MC903-treated mice on day 5 (two-way ANOVA: **p_{genotype} =
511 0.0025, F(2,125) = 6.28; Tukey's multiple comparisons: ****$p_{day\ 5\ WT\ MC903\ vs.\ WT\ EtOH}$ < 0.0001,
512 n=6,8 mice; $p_{day\ 5\ WT\ MC903\ vs.\ KO\ MC903}$ = 0.2198, n=6,6 mice; *$p_{day\ 5\ WT\ EtOH\ vs.\ KO\ MC903}$ = 0.0212, n=8,6
513 mice). **H.** Basophil count from cheek skin of wild-type MC903- and ethanol-treated, and TSLPR^{-}
514 $^{/-}$ MC903-treated mice on day 8 (two-way ANOVA: **p_{genotype} = 0.0023, F(2,117) = 6.38; Tukey's
515 multiple comparisons: ***$p_{day\ 8\ WT\ MC903\ vs.\ WT\ EtOH}$ = 0.0003, n=40,38 mice; ***$p_{day\ 8\ WT\ MC903\ vs.\ KO}$
516 $_{MC903}$ = 0.0003, n=40,15 mice; $p_{day\ 8\ WT\ EtOH\ vs.\ KO\ MC903}$ = 0.5768, n=38,15 mice). For Figures 2G-H,
517 data from days 3, 5, and 8 are presented in **Figure 2-source data table 3. I.** CD4^{+} T cell count
518 from cheek skin of wild-type MC903- and ethanol-treated, and TSLPR$^{-/-}$ MC903-treated mice on
519 day 8 (one-way ANOVA: **p = 0.0053, F(2,24) = 6.564; Tukey's multiple comparisons: *$p_{WT\ MC903}$
520 $_{vs.\ WT\ EtOH}$ = 0.0163, n=11,8 mice; *$p_{MC903\ vs.\ KO\ MC903}$ = 0.0130, n=11,8 mice; $p_{WT\ EtOH\ vs.\ KO\ MC903}$ =
521 0.9953, n=8,8 mice). Wild-type MC903 and EtOH data from **2F-H** are also displayed in **Figure**
522 **1**. Exact values for **Figure 2F-I** displayed in **Figure 2-source data table 3**.

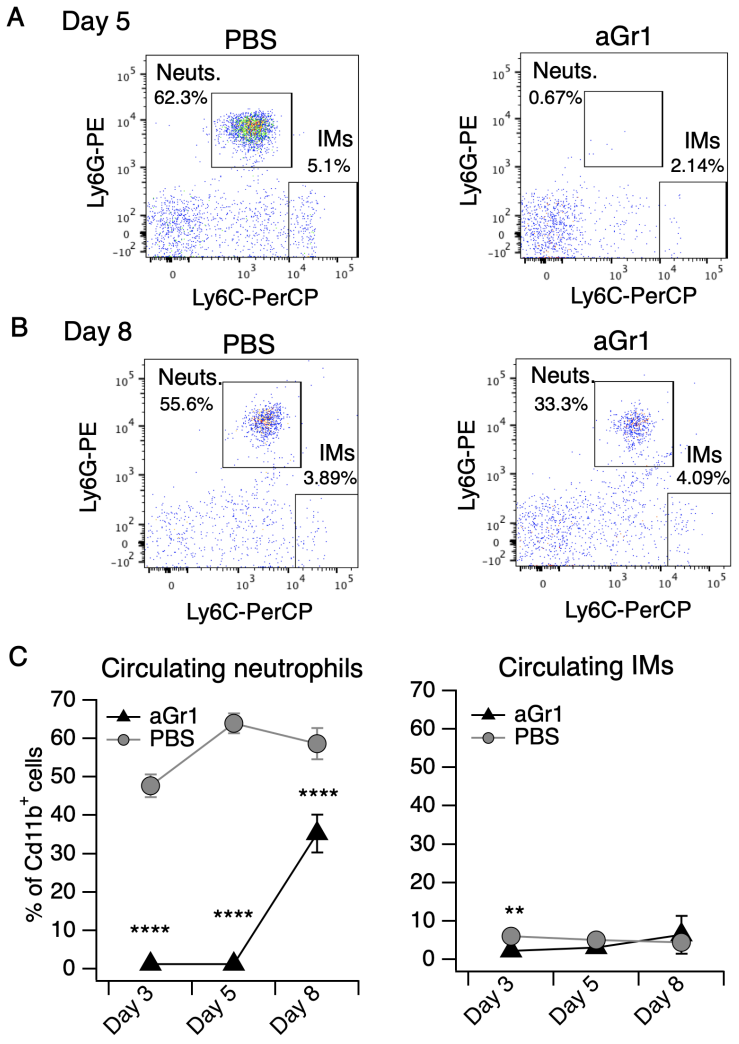

Figure 2-Figure Supplement 1

Figure 2-Figure Supplement 1. aGr1 treatment preferentially depletes neutrophils. A. Representative flow cytometry plots of cells collected from blood of mice injected with PBS or aGr1 (250 µg, i.p.) once-daily for five days concurrent with daily MC903 topical treatment. Shown are $CD45.2^{+}CD11b^{+}$ cells, plotted by Ly6G and Ly6C signal, with neutrophil (Neuts.) and inflammatory monocyte (IMs) populations indicated. Neutrophils were defined as $Cd11b^{+}Ly6G^{+}Ly6C^{mid/high}$ and IMs were defined as $Cd11b^{+}Ly6G^{-}Ly6C^{high}$ (see Methods). **B.** Representative flow cytometry plot as in **A**, depicting neutrophil and IM populations from blood collected on day 8. **C. (Left)** Neutrophil counts in blood shown as % of $Cd11b^{+}$ cells from aGr1/MC903 (black triangles) and PBS/MC903 (gray circles)-treated animals on days 3, 5, and 8 of the model (two-way repeated measures ANOVA: ****$p_{treatment}$ < 0.0001, F(1,31) = 299.5; Sidak's multiple comparisons: ****$p_{day\ 3}$ < 0.0001; ****$p_{day\ 5}$ < 0.0001; ****$p_{day\ 8}$ < 0.0001, n= 16,17 mice). **(Right)** Inflammatory monocyte counts in blood shown as % of $Cd11b^{+}$ cells from aGr1/MC903 and PBS/MC903-treated animals on days 3, 5, and 8 of the model (two-way repeated measures ANOVA: *$p_{treatment}$ = 0.0468, F(1,31) = 4.287; Sidak's multiple comparisons: **$p_{day\ 3}$ = 0.0015; $p_{day\ 5}$ = 0.1918; $p_{day\ 8}$ = 0.2013, n= 16,17 mice). Exact values displayed in **Figure 2-source data table 4**.

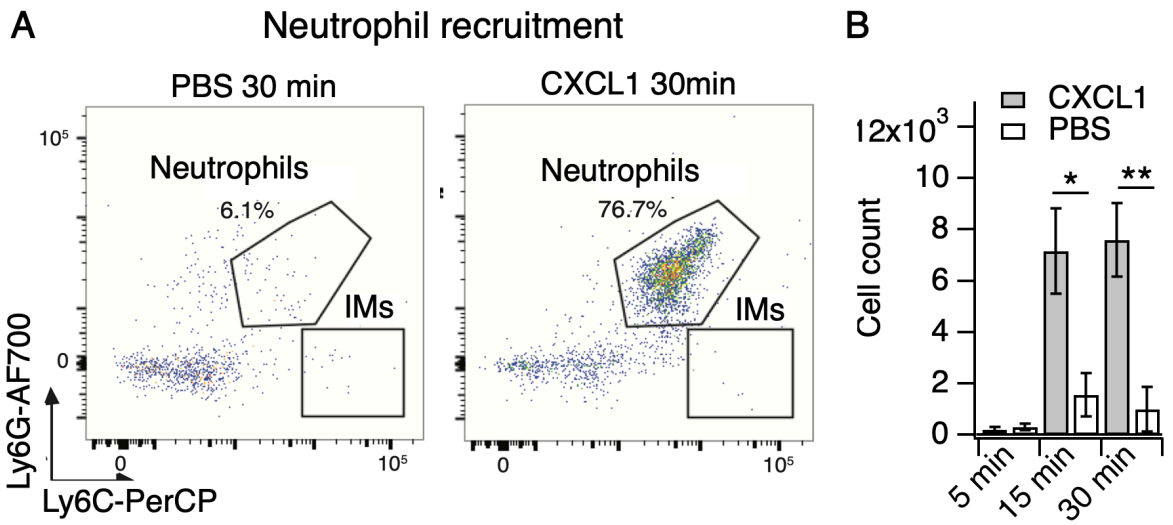

Figure 2-Figure Supplement 2

Figure 2-Figure Supplement 2. CXCL1 rapidly and selectively recruits neutrophils to skin. A. Representative flow cytometry plots of cells from cheek skin of mice injected with PBS or CXCL1 (1 µg, i.d.). Shown are $CD45.2^{+}CD11b^{+}$ cells, plotted by Ly6G and Ly6C signal, with neutrophil and inflammatory monocyte (IM) populations indicated. **B.** Neutrophil count from cheek skin of mice 5, 15, and 30 minutes after injection of CXCL1 or PBS (two-way ANOVA: $^{*}p_{interaction}$= 0.0239, F(2,21) = 4.48; Sidak's multiple comparisons: $p_{5\ min}$ > 0.9999, n=4,5 mice; $^{*}p_{day\ 15\ min}$ = 0.0141, n=4,4 mice; $^{**}p_{day\ 30\ min}$ = 0.0031, n=3,7 mice). Exact values displayed in **Figure 2-source data table 2**.

551

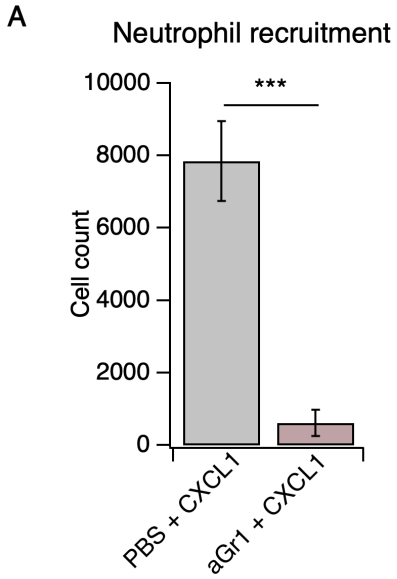

Figure 2-Figure Supplement 3

552
553 **Figure 2-Figure Supplement 3. aGr1 abolishes CXCL1-evoked neutrophil recruitment to**
554 **skin. A.** Neutrophil count from cheek skin of mice 30 minutes after injection of CXCL1 (two-
555 tailed t-test: ***p = 0.0002 (t=4.531, df=19); n=7,14 mice). Mice received either PBS or 250 µg
556 aGr1 approximately 20 hours prior to injection of CXCL1. Exact values displayed in **Figure 2-**
557 **source data table 2**.

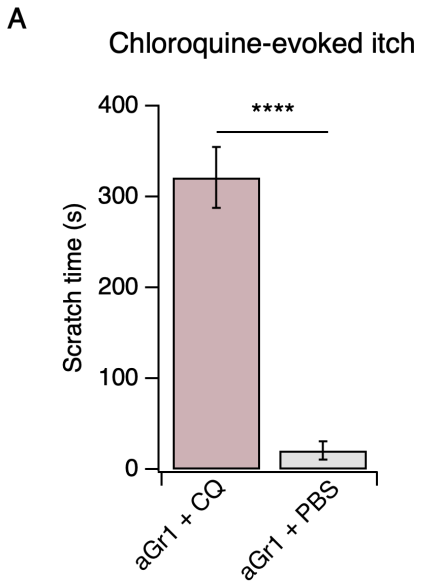

Figure 2-Figure Supplement 4

558
559
560 **Figure 2-Figure Supplement 4. Neutrophil depletion does not affect chloroquine-evoked**
561 **itch. A.** Scratching behavior of mice immediately after injection of chloroquine (CQ) or PBS (i.d.
562 cheek). For neutrophil-depletion experiments, mice received 250 µg anti-Gr1 (aGr1) 20 hours
563 prior to cheek injection of CQ or PBS (two-tailed t-test: ****$p <$ 0.0001 (t=10.58, df=14); n=6,10
564 mice). Exact values displayed in **Figure 2-source data table 2**.
565
566 **Figure 2-source data table 1.** Values displayed in bar plots shown in Figure 2A-D.
567 **Figure 2-source data table 2.** Values displayed in the bar plots shown in Figure 2E and Figs.
568 2-Figure Supplement 2-4.
569 **Figure 2-source data table 3.** Values displayed in the bar plots shown in Figure 2F-I.
570 **Figure 2-source data table 4.** Values used to generate the line plots shown in Figure 2-Figure
571 Supplement 1C.

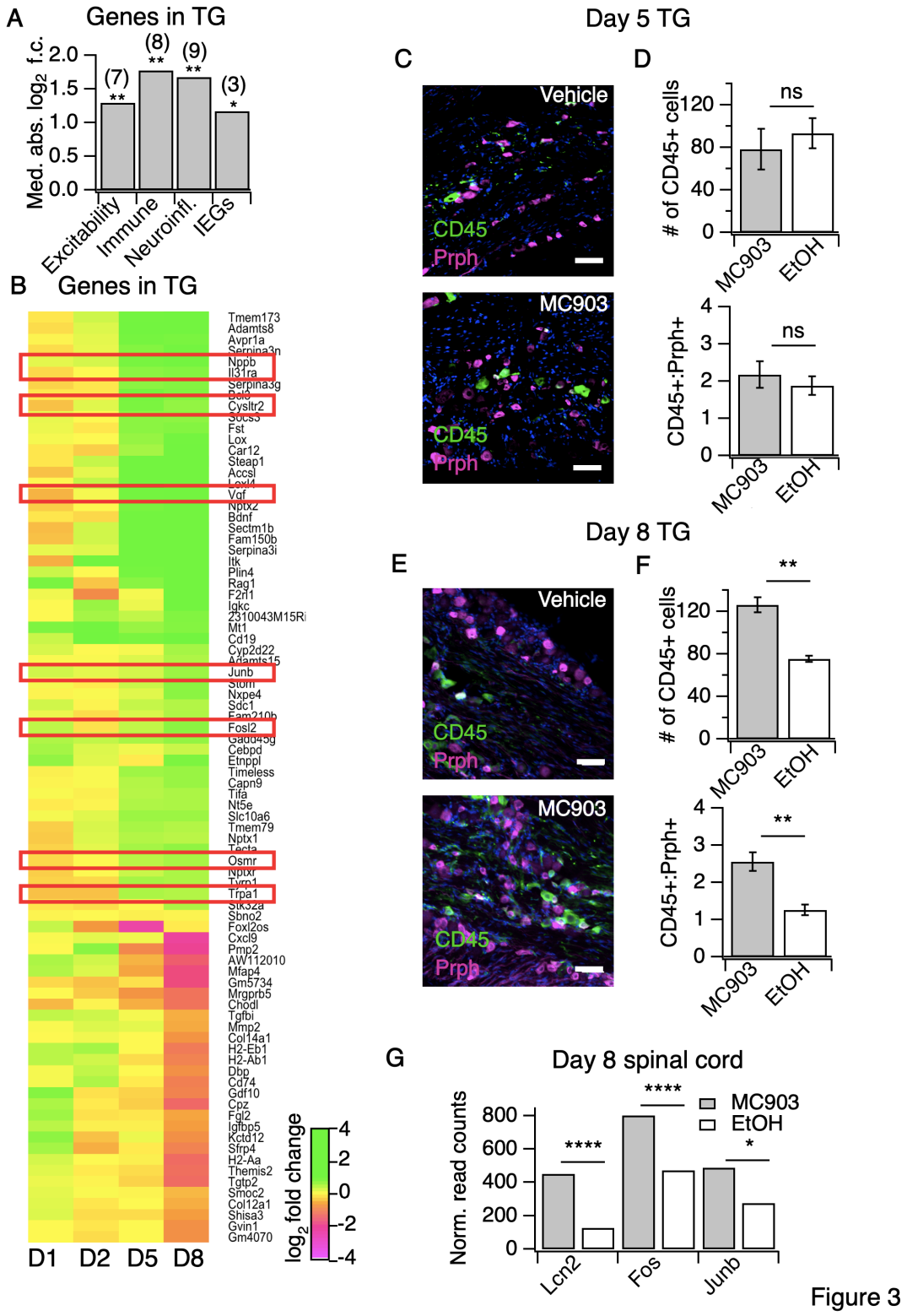

Figure 3

Figure 3. The MC903 model induces rapid and robust changes in neurons. A. Exact permutation test (10,000 iterations, see Methods) for significance of mean absolute $\log_2$ fold change in gene expression at Day 8 (MC903 vs. ethanol) of custom-defined groups of genes for

576 indicated categories (see **Figure 3-source data table 1**). **B.** Log_2 fold change in gene
577 expression (MC903 vs. ethanol) in mouse trigeminal ganglia (TG) at indicated time points for all
578 genes which were significantly differentially expressed for at least one time point in the MC903
579 model. Green bars = increased expression in MC903 relative to ethanol; magenta = decreased
580 expression. Exact values and corrected *p*-values are reported in **Figure 3-source data table 2**
581 and **Supplemental Data**, respectively. **C**. Representative composite images showing immune
582 cells (CD45, green), and sensory neurons (Prph, magenta) with DAPI (blue) in sectioned
583 trigeminal ganglia from mice treated with Vehicle or MC903 for five days on the cheek. **D**.
584 Quantification of images examining average number of $CD45^+$ cells per section and average
585 ratio of CD45:Peripherin cells per section after five days of treatment (p = 0.562 (t=0.6318,
586 df=4), 0.542 (t=0.6660, df=4); two-tailed unpaired t-tests, n=33-159 fields of view (images) each
587 of both trigeminal ganglia from 3 mice per condition treated bilaterally). **E.** Representative
588 composite images showing immune cells (CD45, green), and sensory neurons (Peripherin
589 (Prph), magenta) with DAPI (blue) in sectioned trigeminal ganglia from mice treated with Vehicle
590 or MC903 for eight days on the cheek. **F**. Quantification of images examining average number
591 of $CD45^+$ cells per section and average ratio of CD45:Peripherin cells per section after eight
592 days of treatment (**p = 0.0019 (t=5.977,df=5), **p = 0.0093 (t=4.107,df=4); two-tailed unpaired
593 t-tests; n=42-172 fields of view (images) each of both trigeminal ganglia from 3 EtOH or 4
594 MC903 animals treated bilaterally). Scale bar = 100 µm. Images were acquired on a
595 fluorescence microscope using a 10x air objective. Values from bar plots and all TG IHC data
596 are available in **Figure 3-source data table 3**. **G.** Log_2 fold change in gene expression (MC903
597 vs. ethanol) in mouse spinal cord on day 8 showing selected differentially expressed genes
598 ($p_{adjusted}$ < 0.05). Exact values and corrected *p*-values are reported in **Supplemental Data**.

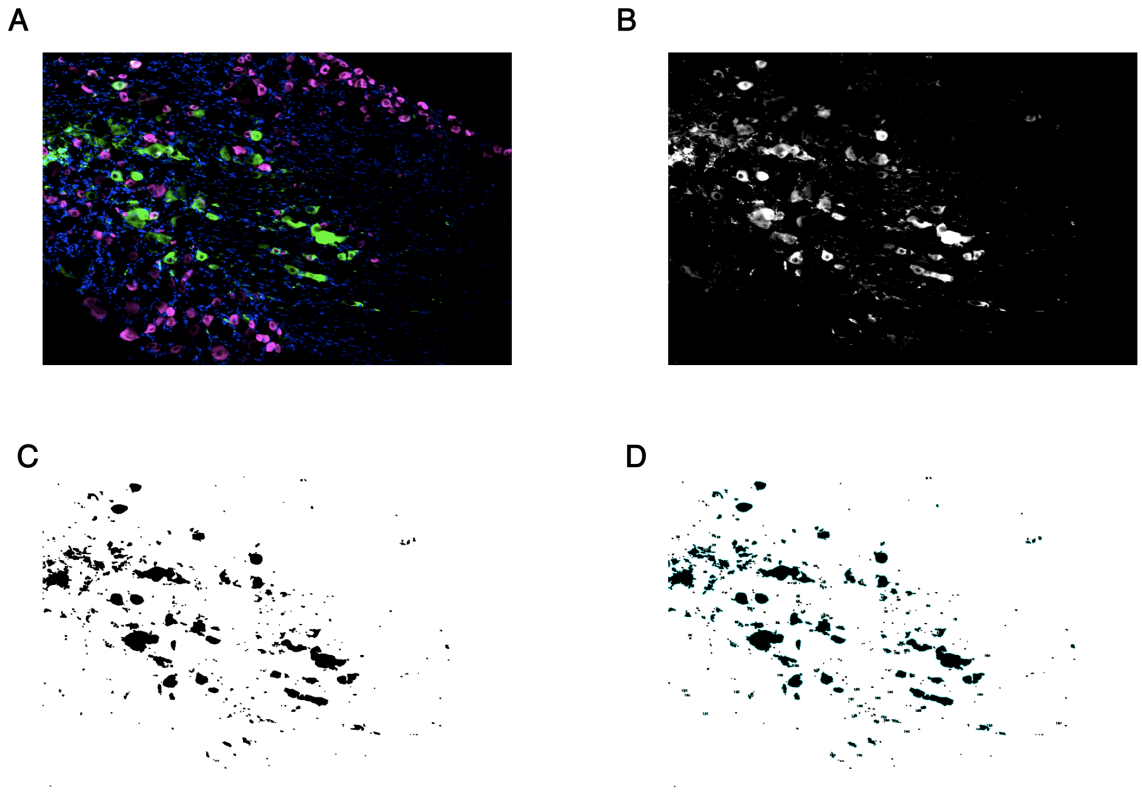

Figure 3-Figure Supplement 1

Figure 3-Figure Supplement 1. Method of image quantification for sectioned trigeminal ganglia. **A.** Representative composite image showing CD45 (green), Peripherin (magenta), and DAPI (blue). **B.** Single-channel CD45 image with automated min/max intensity thresholding. **C.** Resultant binary image generated from **B. D.** Cells were counted as the number of regions of interest (ROIs) outlined in blue.

Figure 3-source data table 1. Values displayed in the bar plot shown in Figure 3A.
Figure 3-source data table 2. Values displayed in the heat map shown in Figure 3B.
Figure 3-source data table 3. Quantification of all IHC samples from trigeminal ganglia, and Values displayed in the bar plots shown in Figure 3D,F.

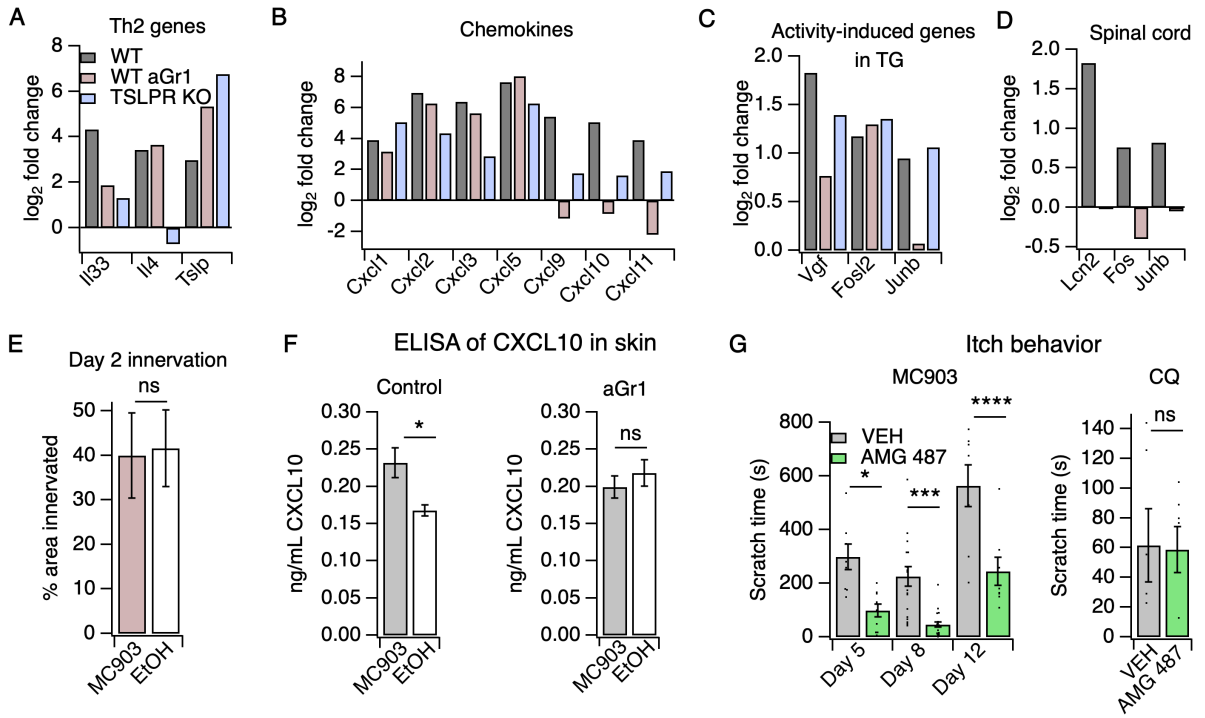

Figure 4. Neutrophils are required for induction of the itch-inducing chemokine CXCL10. **A.** Log_2 fold change (Day 8 MC903 vs. EtOH) of Th2 genes in skin from uninjected wild-type, aGR1-treated, and $TSLPR^{-/-}$ animals. **B.** Log_2 fold change (Day 8 MC903 vs. EtOH) of chemokine genes in skin from uninjected wild-type, aGr1-treated, and $TSLPR^{-/-}$ animals. **C.** Log_2 fold change (Day 8 MC903 vs. EtOH) of activity-induced genes in trigeminal ganglia from uninjected wild-type, aGr1-treated, and $TSLPR^{-/-}$ animals. **D.** Log_2 fold change (Day 8 MC903 vs. EtOH) of *Lcn2* and activity-induced genes in spinal cord from uninjected and aGr1-treated wild-type mice on day 8. For **Figure 4A-D**, exact values and corrected *p*-values are reported in **Supplemental Data. E.** Quantification of innervation (see Methods) of MC903 and EtOH-treated mouse skin as determined from BTIII staining (p = 0.8985; two-tailed t-test (t =0.1294; df =18); n = 9,11 images each from 2 mice per treatment. Exact values are reported in **Figure 4-source data table 1**. **F.** CXCL10 levels in skin homogenate as measured by ELISA on day 8 of the MC903 model for uninjected animals (left; *p = 0.029 (t=2.715, df=7); two-tailed t-test; n = 4,5 animals) and animals which received aGr1 for 8 days (right; p = 0.43 (t=0.815, df=11); two-tailed t-test; n = 6,6 animals). Homogenates were isolated on separate days and so uninjected samples were not compared to aGr1-treated samples. **G.** (Left) Time spent scratching over a thirty minute interval on days 5, 8, and 12 of the MC903 model, one hour after mice were injected with either 3.31 mM of the CXCR3 antagonist AMG 487 or vehicle (10% HPCD; 50 µL s.c. in rostral back); (two-way ANOVA: ****$p_{treatment}$ < 0.0001, F(1,67) = 50.64; Tukey's multiple comparisons: *$p_{day\ 5}$ = 0.0216, n=8,10 mice; ***$p_{day\ 8}$ = 0.0007, n=18,21 mice; ****$p_{day\ 12}$ < 0.0001, n=8,8 mice). (Right) Time spent scratching over a thirty minute interval one hour after mice were injected with either 3.31 mM of the CXCR3 antagonist AMG 487 or vehicle (10% HPCD; 50 µL s.c. in rostral back), and immediately after mice were injected with 50 mM chloroquine (20 µL i.d., cheek). p = 0.92 (t=0.0964, df=8); two-tailed t-test; n = 5,5 mice. Values from bar plots in Figs. 4F-G are displayed in **Figure 4-source data table 2**.

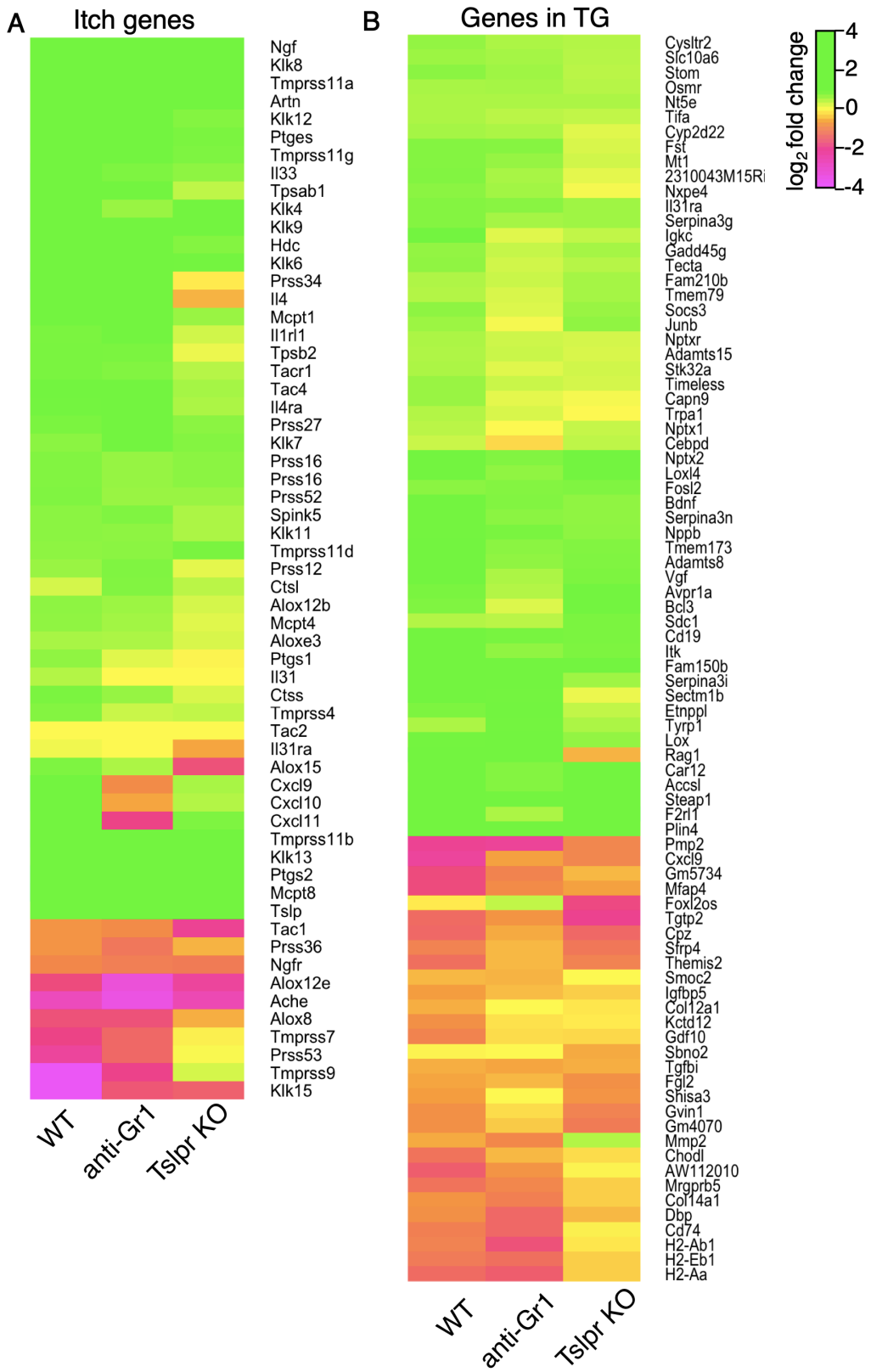

Figure 4-Figure Supplement 1

637

638 **Figure 4-Figure Supplement 1. MC903-dependent gene expression changes in aGr1-**
639 **treated and TSLPR$^{-/-}$ animals. A.** Heat map showing log_2 fold change in gene expression (Day
640 8 MC903 vs. EtOH) for itch-associated genes in wild-type, aGr1-treated, and TSLPR$^{-/-}$ skin.
641 Green bars = increased expression in MC903 relative to ethanol; magenta = decreased
642 expression. Exact values and corrected *p*-values are reported in **Figure 4-source data table 3**
643 and **Supplemental Data**, respectively. **B.** Heat map showing log_2 fold change in gene
644 expression (Day 8 MC903 vs. EtOH) for wild-type, aGr1-treated, and TSLPR$^{-/-}$ mouse trigeminal
645 ganglia (TG) at indicated time points for all genes which were significantly differentially
646 expressed for at least one time point in the MC903 model (See **Figure 2D**). Green bars =
647 increased expression in MC903 relative to ethanol; magenta = decreased expression. Exact
648 values and corrected *p*-values are reported in **Figure 4-source data table 4** and **Supplemental**
649 **Data**, respectively.
650
651 **Figure 4-source data table 1.** Values displayed in the bar plot shown in Figure 4E.
652 **Figure 4-source data table 2.** Values displayed in the bar plots shown in Figure 4F-G.
653 **Figure 4-source data table 3.** Values displayed in the heat map shown in Figure 4-Figure
654 Supplement 1A.
655 **Figure 4-source data table 4.** Values displayed in the heat map shown in Figure 4-Figure
656 Supplement 1B.

A

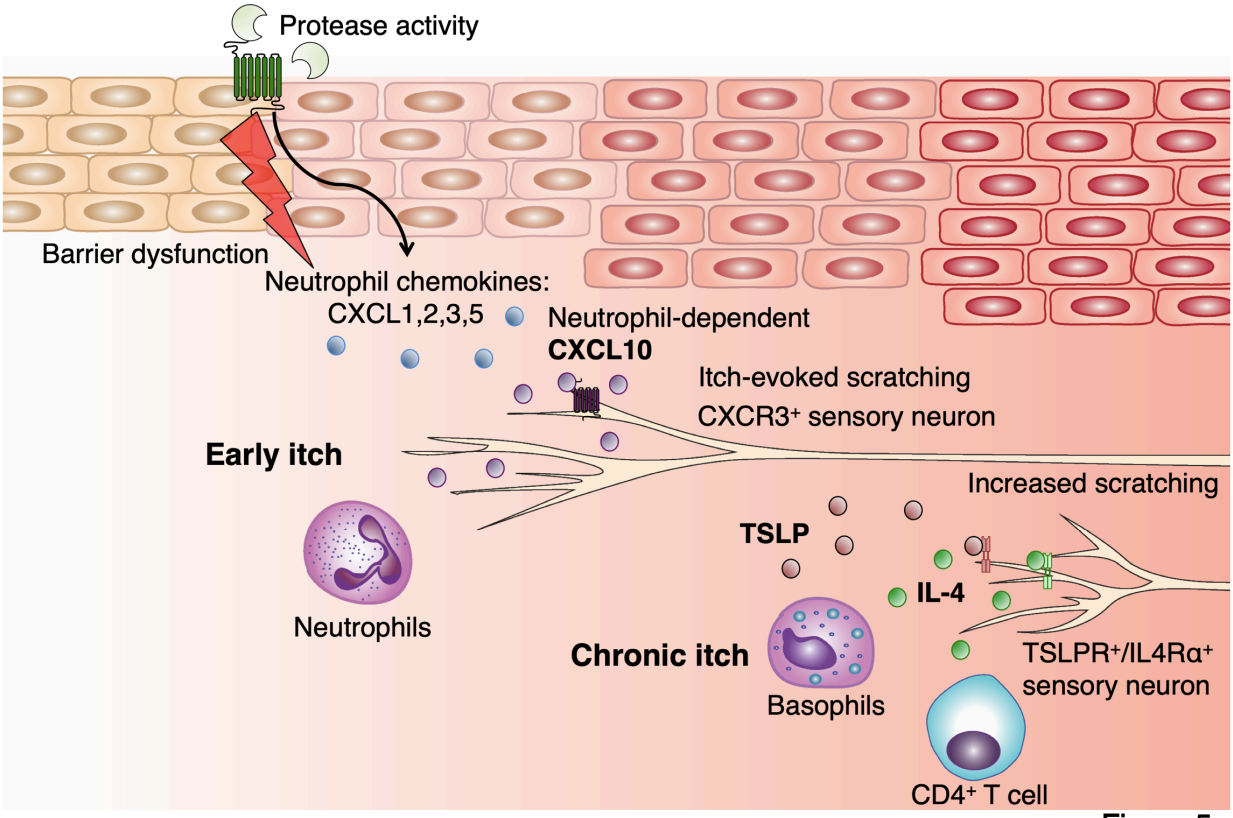

Figure 5

Figure 5. Model of early AD pathogenesis. A. AD induction first results in increased protease expression and barrier dysfunction, which drives production of the cytokines TSLP and CXCL1 via PAR2 activation in keratinocytes. CXCL1 can recruit neutrophils via its receptor CXCR2. Neutrophils may evoke itch by multiple pathways, including degranulation and release of proteases and histamine, production of sensitizing lipids such as PGE_2 and LTB_4, and induction of CXCL10 expression, which can activate sensory neurons via CXCR3. TSLP activates a number of immune cells to elicit IL-4 production, including basophils, which results in increased IL-4, recruitment of $CD4^+$ T cells, and sensitization of neurons to promote itch later in the model (Oetjen et al. 2017).

Supplementary Data - The outputs of all differential expression analyses used to determine adjusted *p* value and log2 fold change for RNA-seq experiments.

672 **Methods**

673 *Mouse studies*

674 All mice were housed in standard conditions in accordance with standards approved by the
675 Animal Care and Use Committee of the University of California Berkeley (12 hr light-dark cycle,
676 21 ˚C). Wild-type C57Bl6 mice were obtained from Charles River or Jackson Laboratories or
677 raised in-house. TSLPR$^{-/-}$ mice were kindly provided by Dr. Steven Ziegler (*Crlf2*^{tm1Jni}; (Carpino
678 et al., 2004) and were backcrossed onto C57Bl6. All experiments were performed under the
679 policies and recommendations of the International Association for the Study of Pain and
680 approved by the University of California Berkeley Animal Care and Use Committee. Genotypes
681 were assessed using standard PCR.
682

683 *MC903 model of atopic dermatitis*

684 MC903 (R&D Systems) was applied to the mouse cheek (20 µl of 0.2 mM in ethanol) once per
685 day for 1-12 days. 100% ethanol was used as a vehicle control. 3-7 days prior to the beginning
686 of treatment, mice were singly housed and their cheeks were shaved. All MC903 studies were
687 performed on 8-12 week old age-matched mice. Behavior, RNA-seq, flow cytometry, and
688 immunohistochemistry were performed on days 1, 2, 3, 5, 8 and/or 12. Behavioral scoring was
689 performed while blind to experimental condition and mouse genotype. Itch behavior was scored
690 for the first 30 min. For AMG 487 experiments in the MC903 model, 50 µL 3.31 mM AMG 487
691 (Tocris) or 20% HPCD-PBS vehicle was injected subcutaneously one hour prior to recording
692 behavior (Qu et al., 2015). Both bout number and length were recorded.
693

694 *MC903 RNA isolation and sequencing*

695 At Days 1 (six hours post-treatment), 2, 5, and 8 post-treatment, mice treated with MC903 or
696 vehicle were euthanized via isoflurane and cervical dislocation. Cheek skin was removed, flash-
697 frozen in liquid nitrogen, and cryo-homogenized with a mortar and pestle. Ipsilateral trigeminal
698 ganglia were dissected and both skin and trigeminal ganglia were homogenized for three
699 minutes (skin) or one minute (TG and spinal cord) in 1 mL RNAzol RT (Sigma-Aldrich). Thoracic
700 spinal cord was dissected from mice treated with 40 µL MC903 or ethanol on the shaved rostral
701 back and homogenized in 1 mL RNAzol. Large RNA was extracted using RNAzol RT per
702 manufacturer's instructions. RNA pellets were DNase treated (Ambion), resuspended in 50 µL
703 DEPC-treated water, and subjected to poly(A) selection and RNA-seq library preparation (Apollo
704 324). Single-end read sequencing (length = 50 bp) was performed by the QB3 Vincent G.
705 Coates Genomic Sequencing Laboratory (UC Berkeley) on an Illumina HiSeq4000. See
706 **Supplementary Table 1** for number of mice per experimental condition and number of mapped
707 reads per sample.
708

709 *MC903 RNA sequencing analysis*

710 Reads were mapped to the mm10 mouse genome using Bowtie2 and Tophat (Langmead and
711 Salzberg, 2012; Langmead et al., 2009). For a given time point, replicate measurements for
712 each gene from treated and control mice were used as input for DESeq (R) and genes with
713 $p_{adjusted} < 0.05$ (for skin and spinal cord) or $p_{adjusted} < 0.1$ (for trigeminal ganglia) for at least one
714 time point were retained for analysis (Anders and Huber, 2010). For the skin dataset, we
715 collated a set of AD-related immune cell markers, cytokines, atopic dermatitis disease genes,
716 neurite outgrown/axonal guidance genes, and locally expressed neuronal transcripts, and from
717 this list visualized genes that were significantly differentially expressed for at least one time
718 point. For the trigeminal ganglia dataset, we plotted all genes that were significantly differentially
719 expressed for at least one time point. Genes from these lists were plotted with clustering using
720 heatmap2 (R).
721

722 *Custom gene groups*

723 Genes were clustered into functional groups and significance was evaluated using a
724 permutation test. Briefly, we first tabulated the absolute value of the $\log_2$ fold change of gene
725 expression (between MC903 and EtOH) of each gene in a given group of *n* genes in turn, and
726 then we calculated the median of these fold change values, z_{true}. We then drew *n* random genes
727 from the set of all genes detected in the samples and computed the median $\log_2$ fold change as
728 above using this null set, z_{null}. Repeating the latter 10,000 times established a null distribution of
729 median $\log_2$ fold change values; we took the proportion of resampled gene groups that exhibited
730 ($z_{true} \geq z_{null}$) as an empirical *p*-value reporting the significance of changes in gene expression for
731 a given group of *n* genes.
732
733 *Flow Cytometry*
734 Skin samples were collected from the cheek of mice at the indicated time points with a 4- or 6-
735 mm biopsy punch and minced into smaller pieces with scissors. Myeloid cells were digested for
736 1h at 37 ˚C using Liberase (Roche)**.** At the end of the digestion, cells were washed in FACS
737 buffer (PBS with 0.5% FCS and 2 mM EDTA). Cells were stained with LIVE/DEAD fixable stain
738 Aqua (Invitrogen), then blocked with anti-CD16/32 (UCSF Core) and stained with fluorophore-
739 conjugated cKit-Biotin (ACK2) (secondary stain with SA-FITC), anti-CD11b-PB (M1/70), Ly6C-
740 PerCP (HK1.4), CD49b-PECy7 (DX5), CD45.2-APCCy7 (104), FceRI-PE (MAR-1), Ly6G-
741 AF700 (1A8, all from eBiosciences). 10ml of counting beads (Invitrogen) were added after the
742 last wash to measure absolute cell counts. $CD4^+$ T cells were digested for 30 minutes at 37˚C
743 using Collagenase VIII (Sigma). At the end of the digestion, cells were washed in RPMI buffer
744 (RPMI, 5% FCS, 1% penicillin-streptomycin, 2 mM L-glutamine, 10 mM HEPES buffer, 1 mM
745 sodium pyruvate). Cells were blocked with antiCD16/32 (UCSF Core) and stained with anti-
746 CD45-APC780 (30-F11; eBiosciences), Cd11b-PECy7 (M1/70; BD Biosciences), B220-PECy7
747 (RA3-6B2; Tonbo Biosciences), Cd11c-PECy7 (N418; eBiosciences), CD3-FITC (145-2C11;
748 eBiosciences), CD8-BV785 (53-6.7; Biolegend), CD4-PE (GK1.5; BD Biosciences), 647-gdTCR
749 (GL3; Biolegend). 10ml of counting beads (Invitrogen) were added after the last wash to
750 measure absolute cell counts, and samples were resuspended in DAPI LIVE/DEAD (Invitrogen).
751 Single cell suspensions were analyzed on an LSR II or LSR Fortessa (BD Biosciences), and
752 data were analyzed using FlowJo (TreeStar, v.9.9.3) software. One skin sample was excluded
753 from analysis due to clear blood contamination.
754
755 *Human keratinocyte RNA sequencing*
756 Normal human epidermal keratinocytes from juvenile skin (PromoCell #C-12001) were cultured
757 in PromoCell Keratinocyte Growth Medium 2 and passaged fewer than 5 times. Cells were
758 treated for three hours at room temperature with 100 μM SLIGRL or vehicle (Ringer's + 0.1%
759 DMSO). Total RNA was extracted by column purification (Qiagen RNeasy Mini Kit). RNA was
760 sent to the Vincent J. Coates Sequencing Laboratory at UC Berkeley for standard library
761 preparation and sequenced on an Illumina HiSeq2500 or 4000. Sequences were trimmed
762 (Trimmomatic), mapped (hg19, TopHat) and assigned to transcripts using htseq-count.
763 Differential gene expression was assessed using R (edgeR).
764
765 *IHC of whole-mount skin*
766 Staining was performed according to Hill et al. (Hill et al., 2018). Briefly, 8-week-old mice were
767 euthanized and the cheek skin was shaved and tape-stripped. The removed skin was fixed
768 overnight in 4% PFA, then washed in PBS (3X for 10 min each). Dermal fat was scraped away
769 with a scalpel and skin was washed in PBST (0.3% Triton X-100; 3X for two hours each) then
770 incubated in 1:500 primary antibody (Rabbit anti beta-Tubulin III: Abcam #ab18207) in blocking
771 buffer (PBST with 5% goat serum and 20% DMSO) for 6 days at 4°C. Skin was washed as
772 before and incubated in 1:500 secondary antibody (Goat anti-Rabbit Alexa 594; Invitrogen
773 #R37117) in blocking buffer for 3 days at 4°C. Skin was washed in PBST, serially dried in

methanol: PBS solutions, incubated overnight in 100% methanol, and finally cleared with a 1:2 solution of benzyl alcohol: benzyl benzoate (BABB; Sigma) before mounting between No. 1.5 coverglass. Sectioned and whole mount skin samples were imaged on a Zeiss LSM 880 confocal microscope with OPO using a 20x water objective. Image analysis was performed using a custom macro in FIJI. Briefly, maximum intensity z-projections of the beta-tubulin III channel were converted to binary files that underwent edge-detection analysis. Regions were defined by circling all stained regions. Region sizes and locations were saved.

IHC of sectioned trigeminal ganglia

TG were dissected from 8 to 12 week old adult mice and post-fixed in 4% PFA for one hour. TG were cryo-protected overnight at 4°C in 30% sucrose-PBS, embedded in OCT, and then cryosectioned at 14 µm onto slides for staining. Slides were washed 3x in PBST (0.3% Triton X-100), blocked in 2.5% horse serum + 2.5% BSA PBST, washed 3X in PBST, blocked in endogenous IgG block (1:10 F(ab) anti-mouse IgG (Abcam ab6668) + 1:1000 Rat anti-mouse CD16/CD32 (UCSF MAB Core) in 0.3% PBST), washed 3X in PBST and incubated overnight at 4°C in 1:1000 primary antibody in PBST + 0.5% horse serum + 0.5% BSA. Slides were washed 3x in PBS, incubated 2 hr at RT in 1:1000 secondary antibody, washed 3X in PBS, and then incubated 30 min in 1:2000 DAPI-PBS. Slides were washed 3x in PBS and mounted in Fluoromount-G with No. 1.5 coverglass. Primary antibodies used: Mouse anti-CD45 (eBioscience #14-054-82) and Chicken anti-Peripherin (Abcam #39374). Secondary antibodies used: Goat anti-Chicken Alexa 594 (ThermoFisher #A11042) and Goat anti-Mouse Alexa 488 (Abcam #150117). DAPI (ThermoFisher #D1306) was also used. Imaging of TG IHC experiments was performed on an Olympus IX71 microscope with a Lambda LS-xl light source (Sutter Instruments). For TG IHC analysis, images were analyzed using automated scripts in FIJI (ImageJ) software. Briefly, images were separated into the DAPI, CD45, and Peripherin channels. The minimum/maximum intensity thresholds were batch-adjusted to pre-determined levels, and adjusted images were converted to binary files. Regions were defined by circling all stained regions with pre-determined size-criteria. Region sizes and locations were saved. All ImageJ macros are available upon request. All scripts are available upon request.

Neutrophil depletion

Neutrophils were acutely depleted using intraperitoneal injection with 250 µg aGR1 in PBS (clone RB6-8C5, a gift from D. Portnoy, UC Berkeley, or Biolegend), 16-24 hours before behavioral and flow cytometry experiments. Depletion was verified using flow cytometry on blood collected post-mortem. For longer depletion experiments using the MC903 model, mice were injected (with 250 µg aGR1 in PBS or PBS vehicle, i.p.) beginning one day prior to MC903 administration and each afternoon thereafter through day 7 of the model, and blood was collected via saphenous venipuncture at days 3, 5, or by decapitation at day 8 to verify depletion.

CXCL10 ELISA measurements in skin

Neutrophil-depleted or uninjected mice were treated with MC903 or ethanol for 7 days. On day 8, 6mm biopsy punches of cheek skin were harvested, flash-frozen in liquid nitrogen, cryo-homogenized by mortar and pestle, and homogenized on ice for three minutes at maximum speed in 0.5 mL of the following tissue homogenization buffer (all reagents from Sigma unless stated otherwise): 100 mM Tris, pH 7.4; 150 mM NaCl, 1 mM EGTA, 1 mM EDTA, 1% Triton X-100, and 0.5% Sodium deoxycholate in ddH2O; on the day of the experiment, 200 mM fresh PMSF in 100% ethanol was added to 1mM, with 1 tablet cOmplete protease inhibitor (Roche) per 50 mL, and 5 tablets PhosSTOP inhibitor (Roche) per 50 mL buffer. Tissues were agitated in buffer for two hours at 4°C, and centrifuged at 13,000 rpm for 20 minutes at 4°C. Supernatants were aliquoted and stored at -80C for less than one week after isolation. After

825 thawing, samples were centrifuged at 10,000 rpm for five minutes at 4°C. Protein content of skin
826 homogenates was quantified by BCA (Thermo Scientific) and homogenates were diluted to 2
827 mg/mL protein in PBS and were subsequently diluted 1:2 in Reagent Diluent (R&D Systems).
828 CXCL10 protein was quantified using the Mouse CXCL10 Duoset ELISA kit (R&D Systems;
829 #DY466-05) according to manufacturer's instructions. Plate was read at 450 nm and CXCL10
830 was quantified using a seven-point standard curve (plus blank and buffer controls) and fitted
831 with a 4-parameter logistic curve.
832
833 *Acute itch behavior*
834 Itch and acute pain behavioral measurements were performed as previously described (Morita
835 et al., 2015; Tsunozaki et al., 2013; Wilson et al., 2013b). Mice were shaved one week prior to
836 itch behavior. Compounds injected: 1 µg carrier-free CXCL1 (R&D systems) in PBS, 3.31 mM
837 AMG 487 (Tocris, prepared from 100 mM DMSO stock) in 20% HPCD-PBS, 50 mM
838 Chloroquine diphosphate (Sigma) in PBS (Chloroquine, CXCL1), along with corresponding
839 vehicle controls. Acute pruritogens were injected using the cheek model (20 µL, i.d.) of itch, as
840 previously described (Shimada and LaMotte, 2008). AMG 487 (50 µL) or vehicle was injected
841 s.c. into the rostral back skin one hour prior to recording of behavior (Qu et al 2015). Behavioral
842 scoring was performed as described above.
843
844 *Lipidomics*
845 Skin was collected from the cheek of mice post-mortem with a 6-mm biopsy punch and
846 immediately flash-frozen in liquid nitrogen. Lipid mediators and metabolites were quantified via
847 liquid chromatography-tandem mass spectrometry (LC-MS/MS) as described before (Moltke et
848 al., 2012; Sapieha et al., 2011). In brief, skin was homogenized in cold methanol to stabilize lipid
849 mediators. Deuterated internal standards (PGE_2-d4, LTB_4-d4, 15-HETE-d8, LXA_4-d5, DHA-d5,
850 AA-d8) were added to samples to calculate extraction recovery. LC-MS/MS system consisted of
851 an Agilent 1200 Series HPLC, Luna C18 column (Phenomenex, Torrance, CA, USA), and AB
852 Sciex QTRAP 4500 mass spectrometer. Analysis was carried out in negative ion mode, and
853 lipid 30 mediators quantified using scheduled multiple reaction monitoring (MRM) mode using
854 four to six specific transition ions per analyte.
855
856 *Statistical analyses*
857 Different control experimental conditions (*e.g.* uninjected versus PBS-injected animals) were
858 pooled when the appropriate statistical test showed they were not significantly different
859 (**Supplementary Table 2**). For all experiments except RNA-seq (see above), the following
860 statistical tests were used, where appropriate: Student's t-test, one-way ANOVA with Tukey-
861 Kramer post hoc comparison, and two-way ANOVA with Tukey Kramer or Sidak's post-hoc
862 comparison. Bar graphs show mean ± SEM. Statistical analyses were performed using PRISM
863 7 software (GraphPad). For all p values, *=0.01<p<0.05, **=0.001<p<0.01,
864 ***=0.0001<p<0.001, and ****=p<0.0001.
865
866 **Acknowledgements**
867 The authors would like to thank members of the Bautista and Barton labs for helpful discussions
868 on the data. We are grateful to S. Ziegler (Ben Aroya Research Institute) for the gift of the
869 $TSLPR^{-/-}$ mouse. We also thank M Pellegrino and L. Thé for pilot studies on human keratinocyte
870 transcriptome analyses and S. Ziegler (Ben Aroya Research Institute) for the gift of the $TSLPR^{-/-}$
871 mouse. D.M.B. is supported by the NIH (AR059385, NS07224 (also to R.B.B)) and the Howard
872 Hughes Medical Institute. G.M.B. is supported by the NIH (AI072429, AI063302, AI104914,
873 AI105184) and the Burroughs Wellcome Fund. J.D. was supported by a Long-Term Fellowship
874 from the Human Frontier Science Program (LT-000081/2013-L). K.G. is supported by NIH grant

EY026082. This work used the Vincent J. Coates Genomics Sequencing Laboratory at UC Berkeley, supported by NIH S10 OD018174 Instrumentation Grant.

Conflict of interest statement

The authors declare no conflict of interest.

References

1. Dalgard, F. J. *et al.* The psychological burden of skin diseases: a cross-sectional multicenter study among dermatological out-patients in 13 European countries. *J. Invest. Dermatol.* **135,** 984–991 (2015).
2. Matterne, U. *et al.* Prevalence, correlates and characteristics of chronic pruritus: a population-based cross-sectional study. *Acta Derm. Venereol.* **91,** 674–679 (2011).
3. Mollanazar, N. K., Smith, P. K. & Yosipovitch, G. Mediators of Chronic Pruritus in Atopic Dermatitis: Getting the Itch Out? *Clin Rev Allergy Immunol* **51,** 263–292 (2016).
4. Berger, T. G., Shive, M. & Harper, G. M. Pruritus in the older patient: a clinical review. *JAMA* **310,** 2443–2450 (2013).
5. Stumpf, A. & Ständer, S. Neuropathic itch: diagnosis and management. *Dermatol Ther* **26,** 104–109 (2013).
6. Mack, M. R. & Kim, B. S. The Itch–Scratch Cycle: A Neuroimmune Perspective. *Trends Immunol.* **39,** 980–991 (2018).
7. Yosipovitch, G. & Bernhard, J. D. Clinical practice. Chronic pruritus. *N. Engl. J. Med.* **368,** 1625–1634 (2013).
8. BS, D. F. C. *et al.* Comparative transcriptomic analyses of atopic dermatitis and psoriasis reveal shared neutrophilic inflammation. *Journal of Allergy and Clinical Immunology* **130,** 1335–1343.e5 (2012).
9. Jabbari, A., Suárez-Fariñas, M., Dewell, S. & Krueger, J. G. Transcriptional profiling of psoriasis using RNA-seq reveals previously unidentified differentially expressed genes. *J. Invest. Dermatol.* **132,** 246–249 (2012).
10. Li, B. *et al.* Transcriptome analysis of psoriasis in a large case-control sample: RNA-seq provides insights into disease mechanisms. *J. Invest. Dermatol.* **134,** 1828–1838 (2014).
11. Suárez-Fariñas, M. *et al.* RNA sequencing atopic dermatitis transcriptome profiling provides insights into novel disease mechanisms with potential therapeutic implications. *J. Allergy Clin. Immunol.* **135,** 1218–1227 (2015).
12. MSc, D. A. E. *et al.* Major differences between human atopic dermatitis and murine models, as determined by using global transcriptomic profiling. *Journal of Allergy and Clinical Immunology* **139,** 562–571 (2017).
13. Guttman-Yassky, E. *et al.* Broad defects in epidermal cornification in atopic dermatitis identified through genomic analysis. *J. Allergy Clin. Immunol.* **124,** 1235–1244.e58 (2009).
14. Nattkemper, L. A. *et al.* The Genetics of Chronic Itch: Gene Expression in the Skin of Patients with Atopic Dermatitis and Psoriasis with Severe Itch. *J Investig Dermatol* **138,** 1311–1317 (2018).
15. Li, M. *et al.* Topical vitamin D3 and low-calcemic analogs induce thymic stromal lymphopoietin in mouse keratinocytes and trigger an atopic dermatitis. *PNAS* **103,** 11736–11741 (2006).
16. Li, M. *et al.* Induction of thymic stromal lymphopoietin expression in keratinocytes is necessary for generating an atopic dermatitis upon application of the active vitamin D3 analogue MC903 on mouse skin. *J. Invest. Dermatol.* **129,** 498–502 (2009).
17. Dai, J., Choo, M.-K., Park, J. M. & Fisher, D. E. Topical ROR Inverse Agonists Suppress Inflammation in Mouse Models of Atopic Dermatitis and Acute Irritant Dermatitis. *J Investig Dermatol* **137,** 2523–2531 (2017).

18. Moosbrugger-Martinz, V., Schmuth, M. & Dubrac, S. in *Inflammation* (eds. E Clausen, B. & Laman, J. D.) **1559,** 91–106 (Springer New York, 2017).
19. Zhang, Z. *et al.* Thymic stromal lymphopoietin overproduced by keratinocytes in mouse skin aggravates experimental asthma. *Proc. Natl. Acad. Sci. U.S.A.* **106,** 1536–1541 (2009).
20. Oetjen, L. K. *et al.* Sensory Neurons Co-opt Classical Immune Signaling Pathways to Mediate Chronic Itch. *Cell* **171,** 217–228.e13 (2017).
21. Morita, T. *et al.* HTR7 Mediates Serotonergic Acute and Chronic Itch. *Neuron* **87,** 124–138 (2015).
22. Li, M. *et al.* Induction of thymic stromal lymphopoietin expression in keratinocytes is necessary for generating an atopic dermatitis upon application of the active vitamin D3 analogue MC903 on mouse skin. *J. Invest. Dermatol.* **129,** 498–502 (2009).
23. Kim, B. S. *et al.* TSLP elicits IL-33-independent innate lymphoid cell responses to promote skin inflammation. *Sci Transl Med* **5,** 170ra16–170ra16 (2013).
24. Kim, B. S. *et al.* Basophils promote innate lymphoid cell responses in inflamed skin. *J. Immunol.* **193,** 3717–3725 (2014).
25. Naidoo, K. *et al.* Eosinophils determine dermal thickening and water loss in a MC903 model of atopic dermatitis. *J. Invest. Dermatol.* (2018).
26. Steinhoff, M. *et al.* Proteinase-activated receptor-2 mediates itch: a novel pathway for pruritus in human skin. *J. Neurosci.* **23,** 6176–6180 (2003).
27. Yosipovitch, G. Dry skin and impairment of barrier function associated with itch - new insights. *Int J Cosmet Sci* **26,** 1–7 (2004).
28. Briot, A. *et al.* Kallikrein 5 induces atopic dermatitis–like lesions through PAR2-mediated thymic stromal lymphopoietin expression in Netherton syndrome. *Journal of Experimental Medicine* **206,** 1135–1147 (2009).
29. Demehri, S., Morimoto, M., Holtzman, M. J. & Kopan, R. Skin-derived TSLP triggers progression from epidermal-barrier defects to asthma. *PLoS Biol.* **7,** e1000067 (2009).
30. Gao, P.-S. *et al.* Genetic variants in thymic stromal lymphopoietin are associated with atopic dermatitis and eczema herpeticum. *J. Allergy Clin. Immunol.* **125,** 1403–1407.e4 (2010).
31. Hidaka, T. *et al.* The aryl hydrocarbon receptor AhR links atopic dermatitis and air pollution via induction of the neurotrophic factor artemin. *Nat. Immunol.* **18,** 64–73 (2016).
32. Tominaga, M. & Takamori, K. Itch and nerve fibers with special reference to atopic dermatitis: Therapeutic implications. *The Journal of Dermatology* **41,** 205–212 (2014).
33. Tominaga, M., Ogawa, H. & Takamori, K. Decreased production of semaphorin 3A in the lesional skin of atopic dermatitis. *Br. J. Dermatol.* **158,** 842–844 (2008).
34. Kou, K. *et al.* Decreased Expression of Semaphorin-3A, a Neurite-Collapsing Factor, is Associated With Itch in Psoriatic Skin. *Acta Derm. Venereol.* **92,** 521–528 (2012).
35. Kamo, A., Tominaga, M., Taneda, K., Ogawa, H. & Takamori, K. Neurotropin inhibits the increase in intraepidermal nerve density in the acetone-treated dry-skin mouse model. *Clin. Exp. Dermatol.* **38,** 665–668 (2013).
36. Haas, S. *et al.* Low density of sympathetic nerve fibers relative to substance P-positive nerve fibers in lesional skin of chronic pruritus and prurigo nodularis. *J. Dermatol. Sci.* **58,** 193–197 (2010).
37. Tominaga, M., Tengara, S., Kamo, A., Ogawa, H. & Takamori, K. Psoralen-ultraviolet A therapy alters epidermal Sema3A and NGF levels and modulates epidermal innervation in atopic dermatitis. *J. Dermatol. Sci.* **55,** 40–46 (2009).
38. Oaklander, A. L. & Siegel, S. M. Cutaneous innervation: Form and function. *J. Am. Acad. Dermatol.* **53,** 1027–1037 (2005).
39. Schüttenhelm, B. N., Duraku, L. S., Dijkstra, J. F., Walbeehm, E. T. & Holstege, J. C. Differential Changes in the Peptidergic and the Non-Peptidergic Skin Innervation in Rat Models for Inflammation, Dry Skin Itch, and Dermatitis. *J. Invest. Dermatol.* **135,** 2049–2057 (2015).

977 40. Pereira, M. P., Mühl, S., Pogatzki-Zahn, E. M., Agelopoulos, K. & Ständer, S. Intraepidermal
978 Nerve Fiber Density: Diagnostic and Therapeutic Relevance in the Management of
979 Chronic Pruritus: a Review. *Dermatology and Therapy* **6,** 509–517 (2016).
980 41. Palmer, C. N. A. *et al.* Common loss-of-function variants of the epidermal barrier protein
981 filaggrin are a major predisposing factor for atopic dermatitis. *Nat. Genet.* **38,** 441–446
982 (2006).
983 42. Gittler, J. K. *et al.* Progressive activation of T(H)2/T(H)22 cytokines and selective epidermal
984 proteins characterizes acute and chronic atopic dermatitis. *J. Allergy Clin. Immunol.* **130,**
985 1344–1354 (2012).
986 43. Mansouri, Y. & Guttman-Yassky, E. Immune Pathways in Atopic Dermatitis, and Definition of
987 Biomarkers through Broad and Targeted Therapeutics. *J Clin Med* **4,** 858–873 (2015).
988 44. Oetjen, L. K. & Kim, B. S. Interactions of the immune and sensory nervous systems in atopy.
989 *FEBS J* **285,** 3138–3151 (2018).
990 45. A role for Th1 and Th2 cells in the immunopathogenesis of atopic dermatitis. 1–3 (1998).
991 46. Hashimoto, T., Rosen, J. D., Sanders, K. M. & Yosipovitch, G. Possible role of neutrophils in
992 itch. *Itch* **3,** e17–6 (2018).
993 47. Dong, X. & Dong, X. Peripheral and Central Mechanisms of Itch. *Neuron* **98,** 482–494
994 (2018).
995 48. Fogh, K., Herlin, T. & Kragballe, K. Eicosanoids in skin of patients with atopic dermatitis:
996 prostaglandin E2 and leukotriene B4 are present in biologically active concentrations.
997 *Journal of Allergy and Clinical Immunology* **83,** 450–455 (1989).
998 49. Ghasemlou, N., Chiu, I. M., Julien, J.-P. & Woolf, C. J. CD11b+Ly6G- myeloid cells mediate
999 mechanical inflammatory pain hypersensitivity. *Proc. Natl. Acad. Sci. U.S.A.* **112,** E6808–
1000 17 (2015).
1001 50. Sivick, K. E. *et al.* Toll-like receptor-deficient mice reveal how innate immune signaling
1002 influences Salmonella virulence strategies. *Cell Host Microbe* **15,** 203–213 (2014).
1003 51. Kim, J. V., Kang, S. S., Dustin, M. L. & McGavern, D. B. Myelomonocytic cell recruitment
1004 causes fatal CNS vascular injury during acute viral meningitis. *Nature* **457,** 191–195
1005 (2009).
1006 52. Shimada, S. G. & LaMotte, R. H. Behavioral differentiation between itch and pain in mouse.
1007 *Pain* **139,** 681–687 (2008).
1008 53. Deftu, A. F., Filippi, A., Gheorghe, R. O. & Ristoiu, V. CXCL1 activates TRPV1 via Gi/o
1009 protein and actin filaments. *Life Sciences* **193,** 282–291 (2018).
1010 54. Deftu, A. F. *et al.* Chemokine (C-X-C motif) ligand 1 (CXCL1) and chemokine (C-X-C motif)
1011 ligand 2 (CXCL2) modulate the activity of TRPV1+/IB4+ cultured rat dorsal root ganglia
1012 neurons upon short-term and acute application. *J. Physiol. Pharmacol.* **68,** 385–395
1013 (2017).
1014 55. Carpino, N. *et al.* Absence of an essential role for thymic stromal lymphopoietin receptor in
1015 murine B-cell development. *Mol. Cell. Biol.* **24,** 2584–2592 (2004).
1016 56. Usoskin, D. *et al.* Unbiased classification of sensory neuron types by large-scale single-cell
1017 RNA sequencing. *Nat. Neurosci.* **18,** 145–153 (2015).
1018 57. Takeda, M., Takahashi, M. & Matsumoto, S. Contribution of the activation of satellite glia in
1019 sensory ganglia to pathological pain. *Neurosci Biobehav Rev* **33,** 784–792 (2009).
1020 58. Solinski, H. J. *et al.* Nppb Neurons Are Sensors of Mast Cell-Induced Itch. *Cell Rep* **26,**
1021 3561–3573.e4 (2019).
1022 59. Scholz, J. & Woolf, C. J. The neuropathic pain triad: neurons, immune cells and glia. *Nat.*
1023 *Neurosci.* **10,** 1361–1368 (2007).
1024 60. Shiratori-Hayashi, M. *et al.* STAT3-dependent reactive astrogliosis in the spinal dorsal horn
1025 underlies chronic itch. *Nat. Med.* 1–8 (2015). doi:10.1038/nm.3912

1026 61. Kanda, N., Shimizu, T., Tada, Y. & Watanabe, S. IL-18 enhances IFN-gamma-induced
1027 production of CXCL9, CXCL10, and CXCL11 in human keratinocytes. *Eur. J. Immunol.*
1028 **37,** 338–350 (2007).
1029 62. Padovan, E., Spagnoli, G. C., Ferrantini, M. & Heberer, M. IFN-alpha2a induces IP-
1030 10/CXCL10 and MIG/CXCL9 production in monocyte-derived dendritic cells and
1031 enhances their capacity to attract and stimulate CD8+ effector T cells. *J. Leukoc. Biol.* **71,**
1032 669–676 (2002).
1033 63. Michalec, L. *et al.* CCL7 and CXCL10 orchestrate oxidative stress-induced neutrophilic lung
1034 inflammation. *The Journal of Immunology* **168,** 846–852 (2002).
1035 64. Ioannidis, L. J. *et al.* Monocyte- and Neutrophil-Derived CXCL10 Impairs Efficient Control of
1036 Blood-Stage Malaria Infection and Promotes Severe Disease. *J. Immunol.* **196,** 1227–
1037 1238 (2016).
1038 65. Tamassia, N. *et al.* Molecular mechanisms underlying the synergistic induction of CXCL10
1039 by LPS and IFN-gamma in human neutrophils. *Eur. J. Immunol.* **37,** 2627–2634 (2007).
1040 66. Koga, C., Kabashima, K., Shiraishi, N., Kobayashi, M. & Tokura, Y. Possible Pathogenic
1041 Role of Th17 Cells for Atopic Dermatitis. *J Investig Dermatol* **128,** 2625–2630 (2008).
1042 67. Qu, L., Fu, K., Yang, J., Shimada, S. G. & LaMotte, R. H. CXCR3 chemokine receptor
1043 signaling mediates itch in experimental allergic contact dermatitis. *Pain* 1–40 (2015).
1044 68. Shalit, M. *et al.* Neutrophil activation in human inflammatory skin reactions. *Journal of*
1045 *Allergy and Clinical Immunology* **80,** 87–93 (1987).
1046 69. Mihm, M. C., Soter, N. A., Dvorak, H. F. & Austen, K. F. The structure of normal skin and the
1047 morphology of atopic eczema. *J Investig Dermatol* **67,** 305–312 (1976).
1048 70. Koro, O., Furutani, K., Hide, M., Yamada, S. & Yamamoto, S. Chemical mediators in atopic
1049 dermatitis: involvement of leukotriene B4 released by a type I allergic reaction in the
1050 pathogenesis of atopic dermatitis. *Journal of Allergy and Clinical Immunology* **103,** 663–
1051 670 (1999).
1052 71. Pinho-Ribeiro, F. A. *et al.* Blocking Neuronal Signaling to Immune Cells Treats Streptococcal
1053 Invasive Infection. *Cell* **173,** 1083–1097.e22 (2018).
1054 72. Sumida, H. *et al.* Interplay between CXCR2 and BLT1 facilitates neutrophil infiltration and
1055 resultant keratinocyte activation in a murine model of imiquimod-induced psoriasis. *J.*
1056 *Immunol.* **192,** 4361–4369 (2014).
1057 73. Cunha, T. M. *et al.* Crucial role of neutrophils in the development of mechanical
1058 inflammatory hypernociception. *J. Leukoc. Biol.* **83,** 824–832 (2008).
1059 74. Carreira, E. U. *et al.* Neutrophils recruited by CXCR1/2 signalling mediate post-incisional
1060 pain. *Eur J Pain* **17,** 654–663 (2013).
1061 75. Kim, N. D. & Luster, A. D. The role of tissue resident cells in neutrophil recruitment. *Trends*
1062 *Immunol.* **36,** 547–555 (2015).
1063 76. Kolaczkowska, E. & Kubes, P. Neutrophil recruitment and function in health and
1064 inflammation. *Nat. Rev. Immunol.* **13,** 159–175 (2013).
1065 77. Wilson, S. R. *et al.* The ion channel TRPA1 is required for chronic itch. *J. Neurosci.* **33,**
1066 9283–9294 (2013).
1067 78. Brunner, P.M. *et al.* The immunology of atopic dermatitis and its reversibility with broad-
1068 spectrum and targeted therapies. *Journal of Allergy and Clinical Immunology* **139,** S65–
1069 S76 (2017).
1070 79. Flier, J. *et al.* Differential expression of CXCR3 targeting chemokines CXCL10, CXCL9, and
1071 CXCL11 in different types of skin inflammation. *J. Pathol.* **194,** 398–405 (2001).
1072 80. Steain, M., Gowrishankar, K., Rodriguez, M., Slobedman, B. & Abendroth, A. Upregulation
1073 of CXCL10 in human dorsal root ganglia during experimental and natural varicella-zoster
1074 virus infection. *J. Virol.* **85,** 626–631 (2011).
1075 81. Liu, B. *et al.* IL-33/ST2 signaling excites sensory neurons and mediates itch response in a
1076 mouse model of poison ivy contact allergy. *PNAS* **113,** E7572–E7579 (2016).

1077 82. Hamilton, J.D. *et al.* Dupilumab improves the molecular signature in skin of patients with
1078 moderate-to-severe atopic dermatitis. *Journal of Allergy and Clinical Immunology* **134,**
1079 1293–1300 (2014).
1080 83. Simpson, E. L. *et al.* Two Phase 3 Trials of Dupilumab versus Placebo in Atopic Dermatitis.
1081 *N. Engl. J. Med.* **375,** 2335–2348 (2016).
1082 84. Yellin, M. *et al.* A phase II, randomized, double-blind, placebo-controlled study evaluating
1083 the efficacy and safety of MDX-1100, a fully human anti-CXCL10 monoclonal antibody, in
1084 combination with methotrexate in patients with rheumatoid arthritis. *Arthritis &*
1085 *Rheumatism* **64,** 1730–1739 (2012).
1086 85. Scott, D. L., Wolfe, F. & Huizinga, T. W. J. Rheumatoid arthritis. *Lancet* **376,** 1094–1108
1087 (2010).
1088 86. Schuttelaar, M. L. A. *et al.* Filaggrin mutations in the onset of eczema, sensitization, asthma,
1089 hay fever and the interaction with cat exposure. *Allergy* **64,** 1758–1765 (2009).
1090 87. Swindell, W. R. *et al.* Genome-wide expression profiling of five mouse models identifies
1091 similarities and differences with human psoriasis. *PLoS ONE* **6,** e18266 (2011).
1092 88. Swindell, W. R. *et al.* RNA-seq identifies a diminished differentiation gene signature in
1093 primary monolayer keratinocytes grown from lesional and uninvolved psoriatic skin. *Sci*
1094 *Rep* **7,** 18045 (2017).
1095 89. Baral, P. *et al.* Nociceptor sensory neurons suppress neutrophil and γδ T cell responses in
1096 bacterial lung infections and lethal pneumonia. *Nat. Med.* **24,** 417–426 (2018).
1097 90. Blake, K. J. *et al.* Staphylococcus aureus produces pain through pore-forming toxins and
1098 neuronal TRPV1 that is silenced by QX-314. *Nature Communications* **9,** 37 (2018).
1099 91. Langmead, B. & Salzberg, S. L. Fast gapped-read alignment with Bowtie 2. *Nat. Methods* **9,**
1100 357–359 (2012).
1101 92. Langmead, B., Trapnell, C., Pop, M. & Salzberg, S. L. Ultrafast and memory-efficient
1102 alignment of short DNA sequences to the human genome. *Genome Biol.* **10,** R25 (2009).
1103 93. Anders, S. & Huber, W. Differential expression analysis for sequence count data. *Genome*
1104 *Biol.* **11,** R106 (2010).
1105 94. Hill, R. Z. *et al.* The signaling lipid sphingosine 1-phosphate regulates mechanical pain. *Elife*
1106 **7,** 702 (2018).
1107 95. Wilson, S. R. *et al.* The epithelial cell-derived atopic dermatitis cytokine TSLP activates
1108 neurons to induce itch. *Cell* **155,** 285–295 (2013).
1109 96. Tsunozaki, M. *et al.* A 'toothache tree' alkylamide inhibits Aδ mechanonociceptors to
1110 alleviate mechanical pain. *J. Physiol. (Lond.)* **591,** 3325–3340 (2013).
1111 97. Moltke, von, J. *et al.* Rapid induction of inflammatory lipid mediators by the inflammasome in
1112 vivo. *Nature Publishing Group* **490,** 107–111 (2012).
1113 98. Sapieha, P. *et al.* 5-Lipoxygenase metabolite 4-HDHA is a mediator of the antiangiogenic
1114 effect of ω-3 polyunsaturated fatty acids. *Sci Transl Med* **3,** 69ra12–69ra12 (2011).
1115